1-1-2018

Biodegradable Nanoparticles In The Treatment Of Cutaneous Malignancy

Emily Sara Yin

Biodegradable nanoparticles in the treatment of cutaneous malignancy

A Thesis Submitted to the
Yale University School of Medicine
in Partial Fulfillment of the Requirements for the
Degree of Doctor of Medicine
and Master of Health Sciences

by
Emily Sara Yin
2018

BIODEGRADABLE NANOPARTICLES IN THE TREATMENT OF CUTANEOUS MALIGNANCY.

Emily S. Yin[1], Julia Lewis[1], Hee-Won Suh[2], Alison Lee[1], Patrick Monico[1], W. Mark Saltzman[2], Michael Girardi[1].

[1] Department of Dermatology, Yale School of Medicine, New Haven, CT

[2] Department of Biomedical Engineering, Yale University, New Haven, CT

ABSTRACT

Keratinocyte-derived carcinomas represent the most common type of malignancy worldwide, and while surgical removal is a first-line therapy, surgery may be impractical for certain patients and does not completely eliminate risk of recurrence. Previous studies have demonstrated the advantages of biodegradable poly(lactic acid)-hyperbranched polyglycerol non-bioadhesive nanoparticles (NNPs) and bioadhesive nanoparticles (BNPs) as chemotherapeutic drug delivery vehicles for the treatment of internal solid tumors. We are now investigating the use of this delivery system for the treatment of cutaneous malignancies, with the goal of maximizing drug efficacy while minimizing systemic effects and treatment-associated morbidity. After topical application of fluorescent dye-loaded NNPs to the intact skin of mice, epidermal penetration of the NNPs to the dermal-epidermal junction and accumulation within hair follicles was observed at time points ranging from 4 to 72 hours. Using the PDV squamous cell carcinoma (SCC) murine model, both dye-loaded NNPs and BNPs exhibited a dose- and time- dependent association with PDV cells *in vitro* by flow cytometry, and BNPs had increased association with cells compared to NNPs. Confocal microscopy confirmed internalization of NPs by cells. Camptothecin (CPT)-loaded NNPs and BNPs were developed; these particles contained 5% by weight CPT. There was no significant difference in effect on PDV cell proliferation *in vitro* among CPT, CPT/NNP, and CPT/BNP treatment groups. A pilot study using subcutaneously transplanted PDV tumors showed effective and complete destruction of the tumor after intratumoral injection of CPT/BNP. A subsequent study using an increased frequency of treatment and lower concentration of CPT compared CPT/intralipid (CPT/IL), CPT/NNP and CPT/BNP injections and showed prolonged survival in all CPT groups compared to control, and a trend toward prolonged survival in NNP and BNP groups compared to CPT/IL. However, none of the three treatments fully eliminated tumor burden in treated mice, suggesting that a higher concentration of drug may be optimal. Overall, our results indicate that both NNPs and BNPs rapidly associate with PDV tumor cells, and *in vitro* drug delivery is not inhibited by NP encapsulation. Further studies are needed to optimize the method, concentration, and frequency of nanoparticle and drug delivery to effectively and consistently treat SCC tumors.

ACKNOWLEDGEMENTS

- To Dr. Michael Girardi, for being an infinitely supportive research mentor, role model, and career advisor, and for creating an encouraging learning environment in which your trainees could thrive. I am inspired by your ability to balance research, medical education, and patient care in your career, seemingly with ease and always with a bright sense of humor. I know that any success in my future career will be in no small part owed to the examples you have set. Thank you for being my greatest advocate and for having faith in me that often exceeded my own.
- To Dr. Julie Lewis, for teaching me virtually everything that I know about lab work and data interpretation. With your endless amounts of expertise, the usually-rough seas of scientific research felt more like smooth sailing. Thank you for your patience and support at all hours of the day. Without your guidance, I could not have accomplished nearly as much as I did.
- To Drs. Mark Saltzman and Hee-Won Suh, for opening up your lab to me and sharing your wealth of knowledge in chemistry and nanoparticle engineering, and for all your efforts in bringing this project to fruition.
- To Patrick Monico, for your innumerable daily contributions in supporting my research work in the lab.
- To Alison Lee, who has worked tirelessly to continue the experiments described within, in the pursuit of a better skin cancer therapy.
- To the residents and faculty of the Yale Department of Dermatology, for your mentorship and commitment to my education and personal success.
- To the Yale School of Medicine and Office of Student Research, including Mae Geter, Donna Carranzo, and Dr. John Forrest, thank you for making my decision to do a research year the easiest choice of my career, and for making this project possible through the National Institutes of Health Clinical and Translational Science Award.
- To my parents, my sister Natalie, and my friends, for supporting me in all my endeavors and keeping me grounded, and without whom this journey could not have been so enjoyable.

TABLE OF CONTENTS

BACKGROUND

Skin cancer epidemiology and treatment

Cancers of the skin are the most common malignancies worldwide. Each year in the US alone, there are over 5.4 million new diagnoses of skin cancer, resulting in over 10,000 deaths.[1–3] Skin cancers may be categorized into melanoma and non-melanoma skin cancers. Non-melanoma skin cancers are further sub-divided into (1) keratinocyte-derived carcinomas (KDCs), which include basal cell carcinoma (BCC) and squamous cell carcinoma (SCC), and (2) non-keratinocyte tumors such as Merkel cell carcinoma and angiocarcinomas of cutaneous vessels, among others. KDCs comprise the vast majority of skin cancer diagnoses, and the incidence of KDCs is rising.[4] Most common in fair-skinned individuals, KDCs largely arise secondary to DNA damage caused by ultraviolet radiation (UVR) exposure, but they may also be triggered by immunosuppression and/or viruses such as human papillomavirus (HPV).[5–8] Both BCCs and SCCs can be destructive via local invasion. SCCs carry an additional risk of metastasis that is estimated at 2-5%, but can be as high as 45% for locally recurrent tumors on the face.[9–13] Actinic keratoses (AK) are precancerous lesions and precursors to SCC, and present as rough, scaly macules on the skin.[14] AKs most commonly arise in fair-skinned individuals with a history of extensive, chronic sun exposure. Fortunately, KDCs are highly curable with early detection and definitive treatment, and treatment can prevent the progression of AKs to cancerous lesions.[15,16]

For many patients with KDCs, in-office surgical procedures are effective first-line treatments. These procedures include conventional excision and Mohs micrographic surgery (MMS). However, surgery may not be appropriate or ideal for all patients. Patients with lesions in areas that are surgically difficult to close, such as on the scalp or face, may require complicated surgical flaps or grafts to achieve acceptable cosmetic results. Grafts may also be associated with complications such as infection and skin discoloration. SCC tumors that cover large surface areas can be seen in patients as a result of severe solar actinic damage, often requiring sizeable excisions that may be destructive, disfiguring, and even functionally debilitating, and they may also necessitate the use of grafts for wound closure. Other patients may prefer alternative, non-surgical methods of treatment for convenience, cost, or other personal preferences.

Notably, KDCs impose a significant cost burden on healthcare systems. Treatment costs of KDCs total over $8.1 billion per year in the US, in large part due to surgical procedures.[17] MMS is a staged excision technique that is most commonly used on the head and neck and involves histopathologic examination after each step of excision in order to maximize the preservation of normal tissue and anatomy and minimize recurrence rates. Despite its lower rates of tumor recurrence, relative to more simple surgical procedures, MMS is particularly costly and time consuming.[18] The average cost of MMS is $1,000-2,000 per treatment, depending on tumor size and number of excision stages.[19,20] Despite these high costs, current surgical treatment methods still do completely eliminate risk of recurrence in vast majority of cases.[21] In light of these limitations,

nonetheless, there is a demand for more cost-effective and clinically practical non-surgical alternatives to improve the treatment of KDCs.

Alternative therapies for skin cancer treatment

Several non-surgical therapies are also available for superficial KDCs; however, these have limited efficacy, a higher rate of recurrence, and are not effective in the treatment of full-depth or invasive KDCs. Radiation therapy may be used for patients who are unwilling or unable to undergo surgery, with a 5-year recurrence rate of 5-20%.[22,23] However, patients may experience significant adverse effects, including radiation dermatitis, epidermal atrophy, and secondary cutaneous malignancies.[24] Radiation therapy is also less favorable for younger patients, as the risk of late-onset adverse effects increases with time. Destruction by curettage and cautery/electrodessication (C&D) involves the removal of the visible tumor by curettage, followed by the use of cautery or electrodessication to destroy 1 mm of tissue at the tumor margins.[25] C&D is recommended only for treatment of small (<1 cm), low-risk KCs, and is associated with 5-year recurrence rates between 3-19%.[26–29]

Cryotherapy, which involves the freezing of skin lesions with liquid nitrogen, is primarily used in the treatment of AKs and superficial KDCs. While the method can be effective in eliminating full-thickness KDCs, its utility is significantly hindered by the inability to assess treatment margins for residual malignanancy.[30–33] Moreover, there is no standardized method of treatment regarding duration and number of cycles of freezing and thawing. Poor cosmetic

outcomes are also of concern, due to common complications including blistering, pigmentary changes, and edema.[25] Post-treatment scar formation can present additional risk due to the potential obscuration of recurrent lesions, and other complications may also include hemorrhage and, rarely, nerve damage.

Diclofenac, ingenol mebutate, and trichloroacetic acid are topical medications that may be used to treat pre-cancerous AKs, but are not sufficiently effective in eliminating KDCs.[34–38] Imiquimod is a topical immunomodulator that stimulates the immune system to react to and destroy tumor cells and may be used in the treatment of superficial KDCs. Topical chemotherapeutic drugs, such as 5-fluorouracil (5-FU), also may also be used to treat superficial KDCs by interfering with DNA synthesis in actively dividing cells.[39]

Similarly, topical photosensitization with δ-aminolevulinic acid (δ-ALA) followed by photodynamic therapy (PDT) can also be used to treat superficial BCCs and SCC in situ.[40] δ-ALA is an amino acid involved in the porphyrin synthesis pathway. It induces photosensitization of epidermal cells via metabolic conversion of δ-ALA to protoporphyrin IX, which accumulates in the skin and produces a cytotoxic photodynamic reaction. However, δ-ALA/PDT is associated with pain, and disease recurrence rates may exceed 50%.[41–43] Pulsed dye laser surgery has been reported as an alternative treatment for BCCs and SCCs, but it is not FDA-approved for this indication and is less effective than surgery.[44,45] Thus, while these non-surgical treatments have some efficacy, they may not be appropriate for deeper or invasive lesions, and success rates may be significantly less than that of surgical treatments.

Despite the abundance of FDA-approved chemotherapeutic agents, 5-FU is the only commonly used chemotherapy in the topical treatment of KDCs. There are a number of challenges that limit the efficacy and practicality of chemotherapeutic drugs for KDC therapy. Small molecule chemotherapeutic agents may rapidly disperse from the application or injection site after administration, resulting in low concentrations of drug at the site of interest. Diffusion into the bloodstream via the dense vasculature within tumors can also lead to significant systemic toxicity. Thus, achieving high local concentrations and efficacy without systemic toxicity is a major concern. Given the efficacy and relative safety of current surgical treatments, a novel chemotherapy-based treatment would need to both be highly effective and have an excellent safety profile to be practical for clinical use. Here, we propose the use of polymer nanoparticles in the delivery of chemotherapeutic agents for the treatment of skin cancer.

Polymer nanoparticles: applications and advantages

Polymer nanoparticles (NPs) is an umbrella term that primarily refers to polymer-based nanospheres and nanocapsules.[46,47] Polymers are commonly used in drug delivery and medical applications due to their favorable biocompatibility and inert nature which result in excellent safety and tolerability. Moreover, NPs have a number of important characteristics that make them attractive and effective for drug delivery. These include the enhanced

permeability and retention (EPR) effect, increased surface area, biodegradability, and controlled-release of drug.

The enhanced permeability and retention (EPR) effect refers to the preferential accumulation of macromolecules and nanoparticles in tumors compared to normal tissue (**Figure 1**).[48–50] The EPR effect occurs due to a combination of irregular tumor vascular structure, high vascular density and permeability, and defective lymphatic drainage.[51,52] In tumor angiogenesis, vascular endothelial cells proliferate out of proportion to pericytes, which are responsible for blood vessel stability. As a result, blood vessels, which normally have junctions less than 10 nm in size, become highly porous with pores greater than 100 nm in diameter.[48] The resulting vascular permeability allows for extravasation of macromolecules such as NPs into the interstitial space of the tumor.[53] In normal tissue, the lymphatic system is able to clear similarly sized macromolecules from the interstitium. However, tumors have impaired lymphatics which prevent effective drainage and may therefore allow the accumulation of NPs in the interstitium and prolonged contact of NPs with tumor cells.[54]

Figure 1. The enhanced permeability and retention (EPR) effect describes the properties of tumor structure that permit the accumulation of macromolecules, such as polymer nanoparticles, in the tumor interstitium. The EPR effect is one of the hypotheses regarding the efficacy of nanoparticles for drug delivery in tumor therapy.

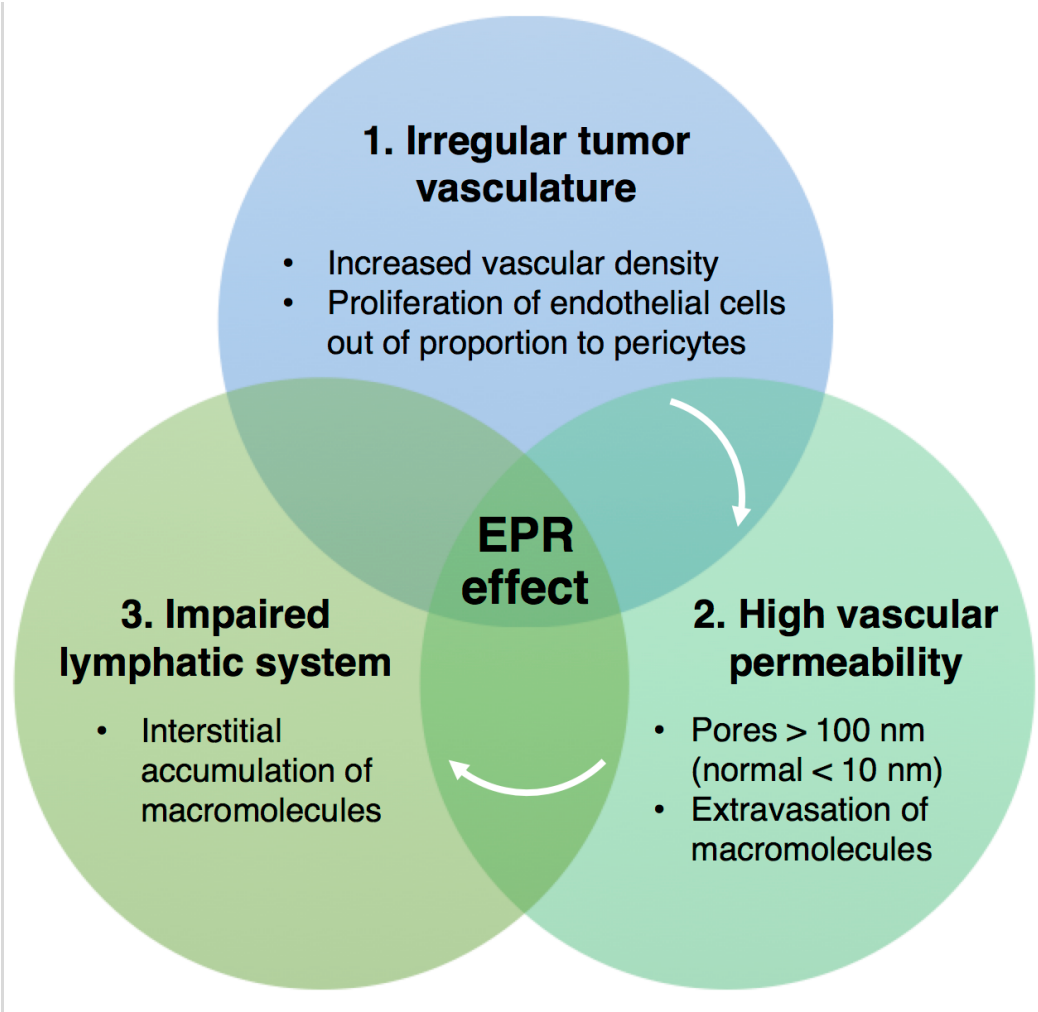

The size of NPs also contributes to reduced systemic toxicity. While the term NP may refer to any particle in the 1-1000 nm size range, NPs are most commonly between 100-500 nm.[47,55] With a diameter larger than that of normal vessel junctions, NPs are typically unable to penetrate normal vasculature, resulting in minimal concentrations of drug reaching normal tissues such as skin, heart, and lung.[51] NPs are primarily removed from the circulation by hepatic excretion and through the mononuclear phagocytic system. They are excreted in the bile and by phagocytosis via Kupffer cells (stellate macrophages) in the liver, macrophages in the spleen, and by local macrophages at the point of entry.[56,57]

The structure of NPs also increases surface area compared to free drug alone. A greater surface area results in an increased likelihood of interaction with other molecules or cells. Modification of the surface of NPs can affect the characteristics and behavior of NPs, and these effects can be amplified by an increased surface area. For instance, antibodies can be used on NPs to target specific cellular proteins and cells, while more non-specific chemical alterations, resulting in more reactive or inert terminal structures, can increase or decrease the likelihood of interactions with cellular proteins.[58–60]

Due to their biodegradable nature, NPs allow for the controlled-release of their contents.[61,62] Notably, nanoparticle controlled release can be attributed to two effects, degradation and erosion. Degradation refers to the chemical reaction of bond-cleavage, while erosion refers to the physical processes of dissolution and diffusion. Poly(esters) such as poly(lactic acid) are chemically degraded by hydrolysis, however it is hypothesized that most biodegradable polymers

undergo breakdown by a combination of both processes.[62] As the polymer degrades over time, encapsulated drug is released from the NPs. Compared with repeated administrations of free drug that would result in alternating peaks and troughs of local concentration, an NP-encapsulated delivery system would provide a sustained release of drug into the surrounding tissue over an extended period of time. The latter results in a more stable local concentration of drug, which can reduce toxicity associated with temporary peaks in concentration. In conjunction with the EPR effect, NPs can also produce a depot effect, allowing for maximal local concentration while minimizing systemic toxicity.

Poly(lactic)-acid (PLA) is a polymer that is commonly used in NPs due to its excellent safety profile, biodegradability, controlled-release, and non-immunogenic properties.[63,64] It can be sourced from renewable resources such as corn starch and sugarcane, among other materials, making it highly sustainable.[65] Given its favorable properties, PLA is used in a variety of medical applications, including implantable screws, plates, and rods.[66–68] In combination with polyglycolic acid, PLA is also used to create dissolvable sutures. Importantly, the surface of polymer NPs can be altered to affect its biochemical properties. Polyethylene glycol (PEG) is a surface coating that was previously commonly used due to its low toxicity and low immunogenicity; however, synthesizing PEG-coated NPs with sufficient density of surface PEG chains can be difficult.[69,70] In this study, we use PLA with a hyper-branched polyglycerol coating (PLA-HPG). While HPG provides similar advantages as PEG in reducing attachment of NPs to cellular proteins, there are a few important distinctions.

HPG is more hydrophilic than PEG, which is advantageous for the encapsulation of poorly soluble, hydrophobic drugs. In addition, the hyperbranched structure of HPG provides enhanced coverage of the NP surface compared to PEG. The multiple hydroxyl groups in HPG also allow for the attachment of multiple ligands per HPG.

While PLA-HPG NPs are relatively inert, incubation of non-bioadhesive NPs (NNPs) with sodium periodate can produce aldehyde-rich NPs, termed bioadhesive NPs (BNPs), which are more biologically reactive. This chemical reaction with sodium periodate involves the conversion of vicinal diols to aldehydes on the surface of NPs.[71] These aldehydes may then readily form covalent bonds, such as Schiff-base bonds, with amines on cellular proteins. The result is improved adhesion of NPs to cell surfaces and subsequently increased uptake by cells. The use of NNPs may result in decreased internalization by cells, while BNPs may enhance internalization via surface interactions.[71]

Use of nanoparticles in therapeutics

Given the aforementioned characteristics, NPs offer a number advantages that are useful for drug delivery. In particular, the use of NPs in cancer therapy has been an important area of study, as chemotherapeutic and cytotoxic anticancer agents often have significant systemic toxicity. A few NP-based cancer therapeutics are already commercially available. Genexol-PM (Samyang Biopharmaceuticals, Seongnam, South Korea) is a polymeric NP micelle formulation for the delivery of paclitaxel to treat metastatic breast cancer. The

NP-based formulation not only decreases the systemic toxicity associated with paclitaxel, but also increases the maximum tolerated dose of paclitaxel to greater than twice that of Taxol.[72–74] Oncaspar (Enzon, Piscataway, NJ, USA) is a modified, PEGylated form of the enzyme L-asparaginase, and is used to treat acute lymphoblastic leukemia.[34] In clinical trials, it reduced the frequency of formation of anti-asparaginase antibodies by hindering detection of the antigen by the immune system.[76,77]

In recent studies from Mark Saltzman's research group, NPs have also been effectively utilized as a drug delivery platform to target difficult-to-treat malignancies in mouse models. To target glioblastoma, Sawyer et al. used polymer NPs containing the chemotherapeutic drug camptothecin in conjunction with convection-enhanced delivery (CED).[78] The efficacy of this combination, which resulted in prolonged survival of glioblastoma-bearing mice, was hypothesized to be a result of an increased duration of exposure to the drug and an increased volume into which drug was distributed via CED. In another study from the same group, Deng et al. determined that BNP-encapsulation of epithilone B enhanced survival of mice with intraperitoneal uterine serous carcinoma tumors, likely due to enhanced interaction with mesothelial cells and improved retention of NPs intraperitoneally.[79]

Murine SCC model and chemotherapeutic drugs

In our assessment of NP efficacy in the treatment of KDCs, we chose to focus our study on SCC, given its relative propensity for metastasis in humans

and increased mortality compared to BCC. In addition, because SCCs can present as widespread lesions that cover large surface areas due to progressive, severe actinic damage or immunosuppression, these cases also stand to benefit the most from a non-surgical therapeutic strategy. We sought an SCC tumor model that could be reliably transplanted, producing tumors that were consistent in size and number. Additionally, our ideal model would produce rapidly progressive tumors, thereby allowing us to most efficiently conduct our experiments. As such, we selected the PDV SCC murine cell line for our study. This cell line was originally derived by chemical carcinogensis via treatment of epidermal cells by 7,12-Dimethylbenz[a]anthracene (DMBA).[80]

Camptothecin (CPT) is a DNA-topoisomerase I inhibitor and powerful cytotoxic agent. CPT is a naturally occurring compound derived from the *Camptotheca acuminata* plant, and it was initially discovered in a screen of plant extracts for antitumor activity.[81] CPT binds to the topoisomerase I and DNA complex resulting in a stable ternary complex that prevents DNA ligation.[82] This results in a double-stranded DNA break and subsequent apoptosis. While CPT analogues such as topotecan and irinotecan have had clinical success, it is not used clinically due to severe adverse effects, including bladder toxicity.[83–85] CPT can have a closed- or open- ring conformation, depending on pH (**Figure 2**). The closed ring or lactone conformation is stable at pH < 5.5 and is the active form of the molecule, while the open ring conformation is more soluble but has poor activity.[86,87] Conversely, bladder toxicity results from exposure of CPT to the low

pH in the urine, which results in a conformational change of CPT to the closed ring form.

We selected CPT for our preliminary studies for two primary reasons. First, it was important for proof of principle that we select a particularly cytotoxic agent to assess whether our delivery system could be effective at altering the bioavailability of the drug. Second, CPT is hydrophobic and poorly soluble, which makes it an excellent candidate for encapsulation using PLA-HPG. While these properties make CPT difficult to use clinically, they are ideal qualities for our study. Encapsulation in NPs may improve the clinical usability of CPT by concentrating its cytotoxic effects locally and decreasing systemic toxicity. Moreover, NP encapsulation may structurally stabilize the drug, delaying inactivation at physiologic pH and enhancing the efficacy of CPT. For similar reasons, we also chose to screen paclitaxel (PTX), a powerful and poorly soluble chemotherapeutic agent that is associated with significant systemic toxicity. As previously mentioned, PTX is not only employed directly as a chemotherapeutic drug, but it is also used in FDA-approved NP-based therapeutics (Genexol-PM).

To study the behavior of NPs in our murine carcinoma model, we encapsulated fluorescent dye in NNPs and BNPs and characterized their association with cultured PDV SCC cells and dispersion after intratumoral injection. We subsequently developed CPT-encapsulated NNPs (CPT/NNP) and BNPs (CPT/BNP) and assessed their cytotoxicity and anti-tumor efficacy in comparison to CPT in vehicle to determine whether NNPs or BNPs may be an effective chemotherapeutic drug delivery platform for the treatment of SCC.

Figure 2. The structure of camptothecin varies depending on the pH of its environment. The active lactone structure (left) is present in acidic solutions, with pH < 5.5. At physiological pH, the inactive open conformation (right) predominates.

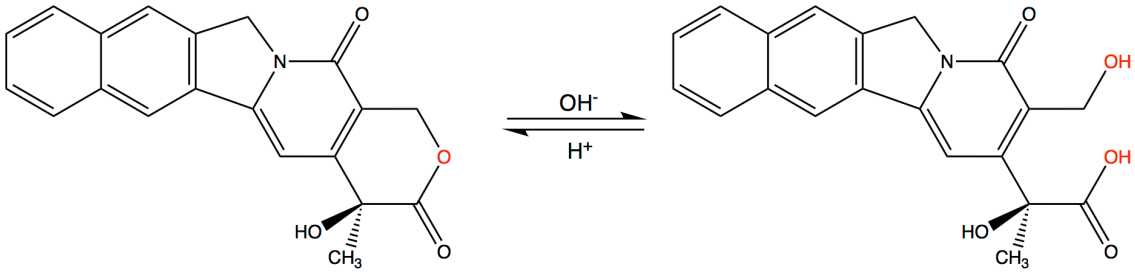

STATEMENT OF PURPOSE

Prior work has shown that NPs may be an effective drug delivery system in the treatment of malignant tumors, and BNPs may be particularly efficacious. This may be due to advantageous properties such as controlled release, depot effect, and increased association with tumor cells compared with non-malignant cells. Our objective is to assess the properties and anti-tumor efficacy of chemotherapy-loaded NPs in a SCC mouse model.

HYPOTHESIS

NP-encapsulation of a chemotherapeutic agent will allow for the safe and effective treatment of cutaneous malignancies by maximizing local concentration of drug and minimizing systemic toxicity and will have superior anti-tumor efficacy compared to chemotherapeutic agent alone due to advantages which include the EPR effect and gradual release of drug. Given their surface properties, BNPs may have superior efficacy compared to NNPs.

SPECIFIC AIMS

1) To characterize NP association with PDV SCC cells and transplanted PDV SCC tumors *in vitro* and *in vivo* using dye-encapsulated NPs
2) To assess the efficacy of chemotherapy-encapsulated NPs in the treatment of established SCC tumors in mice and compare the relative efficacies of drug/NNP, drug/BNP, and drug in vehicle.

METHODS

Synthesis of NNPs and BNPs

Materials. Poly(D,L-lactic acid) (Mw = 20.2 kDa, Mn = 12.4 kDa) was obtained from Lactel Absorbable Polymers (Birmingham, AL). Anhydrous 1,1,1-trishydroxymethylpropane, $KOCH_3$, 10x phosphate-buffered saline (PBS), Na_2SO_3, and $NaIO_4$ were obtained from Sigma Aldrich (Darmstadt, Germany). The 1,10-dioctadecyl-3,3,30,30-tetramethylindodicarbocyanine, 4-chlorobenzenesulphonate salt (DiD) was obtained from Thermo Fisher Scientific (Waltham, MA).

HPG synthesis. HPG was synthesized by anionic polymerization[88]. Briefly, 4.6 mmol 1,1,1-trishydroxymethylpropane (THP) was partially deprotonated by the addition of 1.5 mmol $KOCH_3$ (25% in MeOH) under argon atmosphere at 95ºC for 30 min. The flask was evacuated for 30 min. The system was subsequently refilled with argon, and 25 mL glycidol (x equiv.) was added by syringe pump over 12 hours with stirring. The crude product was then dissolved in methanol, and HPG was precipitated by the addition of acetone. HPG was purified by repeating methanol/acetone precipitation (2x). To remove low molecular weight HPG, HPG was dialyzed against DI water using 0.5-1kDa MWCO dialysis tubing. The water was replaced twice every 12 hours. HPG was precipitated with acetone and dried under vacuum at 80ºC for 12 hours.

PLA-HPG synthesis. PLA (5 g) and HPG (2.15 g) were dissolved in dimethylformamide and dichloromethane (DCM) and dried overnight using 4Å molecular sieves. Subsequently, 0.06 ml N,N'-diisopropylcarbodiimide (DIC) and

10 mg 4-(N,N-dimethylamino)pyridine (DMAP) were added, and the mixture was stirred at room temperature for 5 days. The product was precipitated by adding the solution into cold ether. To purify the product, it was redissolved in DCM and precipitated with cold ether. This precipitate was washed with the cold ether and lyophilized for 2 days.

General methods for NP synthesis. PLA-HPG copolymer (50 mg) was dissolved in 3 mL of solvent mixture (4:1 ethyl acetate:DMSO) with fluorescent dye (DiD, 0.2 wt%) or drug (CPT, 10 wt%). The mixture was added to 4 mL DI water under vortexing and subjected to probe sonication for 3 cycles of 10 seconds each. The emulsion was diluted in 10 ml DI water under stirring and the solvent was evaporated with a rotavapor. The NP suspension was subsequently filtered by centrifugation using an Amicon ultra centrifuge filters (100kDa MWCO). The particles were washed twice with DI water, suspended in DI water, and stored at -20ºC.

Conversion to BNPs. To convert NNPs to BNPs (**Figure 3**), one volume of NNPs at 25 mg/ml was incubated with three volumes of 0.1M $NaIO_4$ (aq) and one volume of 10x PBS for 20 minutes. Three volumes of 0.2 M Na_2SO_3 (aq) were added to quench the reaction. BNPs were washed two times with DI water using Amicon ultra centrifuge filters (100kDa MWCO) and resuspended in DI water. BNPs were stored at 4ºC.

Figure 3. Incubation of non-bioadhesive PLA-HPG nanoparticles (NNP) with $NaIO_4$ produces an aldehyde-rich bioadhesive nanoparticle (BNP). The reaction is quenched using Na_2SO_3, and formaldehyde is formed as a byproduct. Encapsulated drug is illustrated as white circles within the nanoparticles.

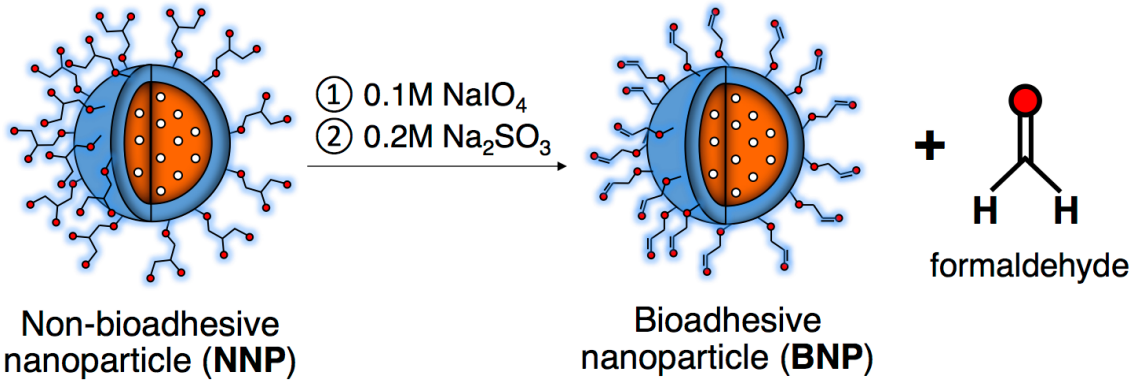

Assessment of NNPs and BNPs. To determine the concentration of NPs, a 100 µl aliquot of NP solution was placed in a pre-weighed 1.5 ml Eppendorf tube, flash-frozen by incubation of the tube in liquid nitrogen, and lyophilized overnight. The Eppendorf tube was subsequently weighed, and the initial weight of the tube was subtracted to determine the weight of the NPs. The amount of DiD or CPT encapsulated was determined by fluorescence. For quantification of CPT, one volume of NPs was diluted in acidified DMSO, volume ratio 1:100 of 1N HCl:DMSO (with SDS to assist dissolution of CPT). A standard curve was prepared using known concentrations of CPT using the same assay. CPT fluorescence was measured by fluorescence spectroscopy, with excitation at 370 nm and emission at 428 nm, and the loading concentration of CPT in NPs was determined by comparison to the standard curve. For DiD, a standard curve was also prepared, with excitation at 644 nm and emission at 665 nm.

Cell lines and cell culture

The PDV squamous cell carcinoma cell line (PDV) was obtained from Allan Balmain (UCSF). PDV cells were maintained in RPMI 1640 medium supplemented with 10% fetal bovine serum (FBS), 2% 1M Hepes, 1% 200mM L-glutamine, 1% 100mM sodium pyruvate, 1% 5 x 10^{-3} M 2-mercaptoethanol, 1% 10mM non-essential amino acids, and 1% 10,000 U/ml-µg/ml penicillin-streptomycin. Live cells were maintained at 37ºC and 5% CO2 in 25 cm^2 or 125 cm^2 Falcon tissue culture flasks (Thermo Fischer Scientific, Waltham, MA, USA). Cells were harvested from flasks using 0.25% Trypsin-EDTA (Thermo Fischer

Scientific). For long-term storage, cells were resuspended in 90% FBS and 10% DMSO and stored at -196ºC in a liquid nitrogen tank.

Confocal microscopy and image processing

All microscopy images were captured using the Leica TCS SP5 confocal microscope. Images were processed using Fiji/ImageJ (NIH, Rockville, MD, USA)[89]. Stacked images consist of images taken at 0.5-2 μm z-intervals. 3D visualizations were constructed using Huygens Professional v17.04 (Scientific Volume Imaging, Hilversum, Netherlands).

Flow cytometry data collection and analysis

Skin, tumor, and lymphatic cells were analyzed by flow cytometry as described below. Samples were matched with the appropriate isotype controls. Stratedigm S1000EX flow cytometer and CellCapture software v3.1 (Stratedigm Inc., San Jose, CA, USA) were used to collect flow cytometry data. Data was analyzed using FlowJo v10.4 (FlowJo LLC, Ashland, OR, USA).

Animal care and mouse tumor model

All animal procedures were performed in accordance with Yale Institutional Animal Care and Use Committee (IACUC). Animals were kept in the Yale Animal Resource Center and given free access to food and water throughout the duration of the study. Mice were anesthetized in an induction chamber using 30% isoflurane (Zoetis, Parsippany-Troy Hills, NJ, USA) in

propylene glycol (Thermo Fischer Scientific). Mice were euthanized by overdose in the same manner at the end of experiments.

Tumor transplantation. TCRβ-/- mice on the C57Bl/6J background were obtained from The Jackson Laboratory (Bar Harbor, ME). To prepare the mice for tumor transplantation, hair over the dorsal right flank was shaved with electric clippers, and shaved skin was cleaned with an alcohol wipe. PDV cells were harvested from tissue culture flasks. Cells were counted and then washed and resuspended in ice-cold PBS at a concentration of 20 million cells/ml. Mice were anesthetized prior to the procedure as described above. A subcutaneous injection of 1 million cells/50 µl was placed using a 27.5-gauge syringe, forming a small bleb at the site of injection.

Preparation for topical application. For topical application of DiD/NNPs, C57Bl/6 mice were shaved using a straight razor blade while hair was in telogen (resting) phase, at approximately 8-9 weeks of age. To minimize inflammation in the skin, experiments were initiated 4-7 days after shaving.

In vitro *PDV cell uptake of NPs*

Cells were seeded at a density of 100,000 per 1.9 cm^2 well in a 24-well tissue culture treated plate (Corning, Inc.). At 24 hours after plating, media was removed by glass pipette, and DiD/NNPs or DiD/BNPs were added at a concentration of 0.01, 0.1, or 1.0 mg/ml in CRPMI. After 6 or 24 hours, cells were washed with PBS and trypsinized. The enzymatic reaction was stopped by addition of CRPMI. Cells were pelleted by centrifuge and washed twice with stain

buffer (1x PBS, 1% FBS, 0.09% NaN3) and subsequent centrifugation. All subsequent steps occurred on ice. Cells were then resuspended in surface block containing anti-FcR (5 µg/ml), normal hamster IgG (11.8 µg/ml), and normal rat IgG (22.2 µg/ml) and incubated for 15 minutes in a round-bottom 96-well plate (Corning, Inc.). Cells were pelleted by centrifugation for 5 minutes at 1100 rpm at 4ºC, and supernatant was discarded. Pellet was resuspended in 100 µl of 2.5 µg/ml FITC anti-mouse CD326 Ep-CAM (BioLegend, San Diego, CA). After 25 minutes incubation, cells were centrifuged and washed twice with 250 µl stain buffer. Cells were pelleted by centrifugation, and supernatant was removed. Cells were resuspended in 100 µl of secondary antibody, 5 µg/ml Alexa-488-anti-FITC (Life Technologies, Thermo Fischer Scientific) for 25 minutes. Centrifugation and washing was repeated twice as described above. Cells were pelleted by centrifugation and resuspended in 1% PFA for 20 minutes. Cells were centrifuged and resuspended in PBS for short-term storage at 4ºC. Cells were adhered to slides for visualization using the CytoSpin 4 Cytocentrifuge (Thermo Fischer Scientific) 800 rpm for 5 minutes. Cells were mounted using ProLong Gold Antifade Mountant with DAPI (Thermo Fischer Scientific) and a coverslip was placed. Slides were kept in the dark at room temperature for 24 hours and subsequently stored at -20ºC.

In vivo topical application

NNPs were thoroughly vortexed before use and diluted to 2 mg/ml using DI water or 5% di(ethylene glycol) ethyl ether (Sigma) in DI water. Mice were

anesthetized as described above. The rectangular area used for testing was marked and measured on the dorsal back, ranging from 1-3 cm in each dimension. NNPs were applied at a density of 2 µl/cm^2 at a concentration of 2 mg/ml. The solution was allowed to dry on the skin for 5 minutes. A second coat of NNPs was subsequently reapplied at the same density and allowed to dry for 5 minutes. The area was occluded using a non-stick bandage and secured in place with tape. At the end point, mice were euthanized. The demarcated area of skin was tape-stripped to remove excess dye on the surface and harvested. Tissue was fixed in 4% methanol-free paraformaldehyde (PFA) for 48 hours and frozen in Tissue-Tek OCT compound (Electron Microscopy Sciences, Hatfield, PA) for sectioning.

***Nanoparticle dispersion after intratumoral injection* in vivo**

Intratumoral injections. PDV tumors were transplanted as described above. Tumors were measured using calipers three times per week beginning 1 week after transplantation. To determine where nanoparticles disperse after intratumoral injection, we injected 100 µl DiD/NNP intratumorally and used flow cytometry to measure fluorescence in individual cells of the tumor and draining inguinal lymph node as described below.

Materials. DNAse was prepared by reconstituting 10 million Dornase units (ICN#190062) in a mixture of 1 ml 10x DNAse buffer, 4 ml sterile distilled water, and 5 ml glycerol. Aliquots of DNAse were stored at -20ºC. Media A was prepared with 100 ml MEM (Gibco, Thermo Fischer Scientific), 10 ml FCS, 1 ml

100x pencillin-streptomycin, and 50 µl DNAse, and stored at 4ºC. Trypsin-GNK was prepared by adding the following to 1700 ml of dH_2O: 14.7 g NaCl, 0.7 g KCl, 1.7 g glucose, and 5.0 g Trypsin (Sigma T-1005). The pH was adjusted to 7.6 using $NaHCO_3$, and the solution was filter sterilized. Trypsin-GNK aliquots were stored at -20ºC. Personna single-edge surgical prep razor blades were obtained from AccuTec Blades Inc. (Verona, VA, USA). Dermis Digestion buffer was prepared fresh by mixing the following into RPMI: 2.7 mg/ml collagenase (Sigma), 0.25 mg/ml hyaluronidase (Sigma), 10 µl/ml DNAse, 10 µl/ml 1 M HEPES (Gibco), and 10 µl/ml 100x sodium pyruvate (Gibco). Nalgene™ Rapid-Flow™ 0.2 µm PES membrane. Petri dishes and centrifuge tubes were obtained from Corning, Inc. (Corning, NY, USA).

Tissue harvesting. Mice were euthanized and affixed to a Styrofoam board. The skin of the mice was soaked with 95% ethanol, covering all areas to be manipulated during tissue harvesting. Hair was removed over the site of the tumor using surgical prep blades. With the mouse in the supine position, a midline cut in the skin was made, running superiorly from the groin to the neck using scissors. Subsequent cuts were made bilaterally from the groin to the inner hind legs, creating flaps on each side of the abdomen that were then pulled outward and affixed to the board. Inguinal lymph nodes, found on these skin flaps, were then dissected away from subcutaneous fat using forceps. Lymph nodes were placed in a dish of Media A on ice. With the mouse in the prone position, the tumor and skin overlying the tumor were resected and prepared as described below. For flow cytometry experiments, the skin was separated from

the tumor. For assessment of histology by confocal microscopy, the skin and tumor were remained attached by subcutaneous fat and/or adhesions.

Epidermal and dermal cell preparation. Skin was placed on a petri dish lid with the epidermis facing down and was spread out until flat. Subcutaneous fat was removed by scraping the dermal side using the dull edge of a pair of closed scissors. A surgical prep blade was then used to cut the skin into approximately 1 cm wide strips. Strips of skin were placed dermal side down in a petri dish containing Trypsin-GNK (T-GNK). The dish was covered and incubated for 2 hr at 37°C. Fine forceps were then used to separate the epidermis from dermis. To digest the epidermis, all epidermal strips from a single mouse were collected and in 50 ml tube containing 8 ml T-GNK, 2 ml RPMI, and 50 µl DNAse. Tubes were incubated in a 37°C shaking water bath for 10 minutes. Tubes were removed from the water bath, and 10 ml Media A was added to each tube. Digested tissue was filtered through 70 um Nitex mesh into a new 50 ml Falcon tube to remove stratum corneum, hairs, and other large debris. Cells were centrifuged and washed with Media A. To digest the dermis, the tissue was first minced in Petri dish containing Dermis Digestion Buffer. Tissue was incubated for 1-1.5 hr at 37°C with occasional mixing using serological pipet to break up clumps. The digested mixture was filtered through 70 µm Nitex nylon mesh to remove any remaining large pieces of tissue. Media A was added to stop digestion of tissue, and cells were washed twice with Media A. For some experiments, epidermal and dermal cells were pooled for analysis.

Lymph node cell preparation. The rough area of two frosted microscope slides (Thermo Fischer Scientific, Waltham, MA, USA) were dipped in a petri dish containing Media A to remove dust. Using forceps, lymph nodes were placed on the frosted area of one slide and covered with the frosted area of the second slide. The two slides were gently rubbed together to break apart the lymph nodes and allow the cells to separate, and free cells were washed into the petri dish from the slide. The media containing lymph node cells was collected and filtered through sterile 70 μm Nitex nylon mesh into a 15 ml Falcon tube. Cells were centrifuged for 8 minutes at 1100 rpm, before resuspension in Media A. The cells were placed on ice.

Spleen preparation. The spleen was minced in Media A using ethanol-sterilized scissors. The media was collected and filtered using a 70 um Nitex mesh into a 15 ml Falcon tube. The collected cells were centrifuged for 8 minutes at 1100 rpm and resuspended in 5 ml ACK lysis buffer. After incubation for 4 minutes, the tube was filled with Media A and centrifuged for another 8 minutes. The pellet was resuspended in Media A and placed on ice.

Tumor cell preparation. Each tumor was placed in a 60-mm petri dish containing collagenase/hyaluronidase buffer and minced using ethanol-sterilized scissors. The tissue was incubated at 37°C for 1.5-2 hr with occasional mixing with serological pipet to break up larger pieces of tissue. Liquid from the dish was moved to a 15 ml Falcon tube, and Media A was added to stop digestion. The suspension was filtered using 70 um Nitex into a new 15 ml Falcon tube. The remaining undigested pieces of tissue were incubated with T-GNK at 37°C for

1.5-2 hr with occasional mixing, until the majority of tissue was digested. Media A was added to stop the digestion, and the cell suspension was filtered through a 70 um Nitex mesh. Cells were pelleted by centrifugation and resuspended in a small amount of Media A for counting and placed on ice. The collagenase/hyaluronidase-digested cells and the T-GNK digested cells were pooled for analysis.

Cell type staining. Cells were counted using a Neubauer Ruled hemocytometer. Up to 1 million cells were aliquoted per FC sample. Cells were resuspended in 50 µl/sample of ice-cold block (stain buffer with anti-FcR (1:100) + normal hamster IgG (1:500) + normal rat IgG (1:500)). Aliquots of 50ul/well were placed into a round bottom 96-well plate on ice and covered with foil to minimize light exposure. Ethidium monoazide bromide (EMA) at 2x concentration was prepared in the dark by mixing 4 ml stain buffer and 2 ul of 2x EMA. For a final concentration of 0.25 µl EMA/ml, 50 µl of 2x EMA was added to indicated samples. The foil and plate cover were removed, and the plate was placed on ice under a fluorescent lamp for 10 minutes. After light exposure, 150 µl of stain buffer was added to each well. The plate was covered and centrifuged for 5 minutes. Supernatant was removed. Cells were resuspended in indicted primary antibody diluted in stain buffer. The plate was covered in foil and incubated on ice for 25 minutes. The plate was centrifuged and washed twice with stain buffer. Cells were pelleted by centrifugation and resuspended in 1% PFA for 20 minutes. Samples were centrifuged and resuspended in PBS before storage at 4ºC until cytometry analysis.

***CPT nanoparticles* in vitro**

Cells were harvested from tissue culture flasks using 0.25% Trypsin-EDTA as described above. Cells were washed using media containing 10% FBS, 1% 10,000 U/ml-µg/ml penicillin-streptomycin, and 10mM Hepes in HBSS. Cells were resuspended in CRPMI and counted. Cells were centrifuged and resuspended at 100 cells/µl and held on ice. Three-fold dilutions of CPT, CPT/NNPs, and CPT/BNPs were prepared, with CPT concentration ranging from 0.002 µM to 15 µM. Cells were plated at a density of 5,000 cells per well in a flat-bottom 92-well tissue culture clear bottom plate. At 24 hr after cell plating, the prepared solutions of CPT, CPT/NNPs, CPT/BNPs, or DMSO (vehicle control) in CRPMI were added to the wells. Cells were incubated at 37 ºC for 24, 48, or 72 hr. After incubation, the CellTiter-Glo® Luminescent Cell Viability Assay (Promega, Madison, WI, USA) was used to determine cell viability based on the quantity of ATP present in each well. Luminescence was read using the Victor Light Luminescence Counter (Perkin Elmer, Waltham, MA, USA). Luminescence was normalized to a vehicle control containing CRPMI and 3% DMSO, the highest concentration of DMSO used in any sample.

***Assessment of chemotherapeutic nanoparticle efficacy* in vivo**

PDV tumors were transplanted in mice as described above. In the pilot experiment of 4 mice, tumors were injected with 0.5 mg CPT/100 µl of CPT/BNPs at 23 days after tumor transplantation. This treatment was repeated at 1 week.

Control mice received two intratumoral injections of 100 µl PBS on the same schedule. Subsequent experiments used a modified injection method to reduce ulceration and minimize potential for systemic toxicity. In these experiments, mice were treated with 0.125 mg CPT/50 µl of CPT/IL, CPT/NNPs, or CPT/BNPs when the diameter of the tumor had reached 3 mm in any dimension. Injections were repeated at a twice-weekly schedule. Injections were not performed on a tumor if one of the following was true: (1) there was no identifiable tumor, or (2) there was open ulceration at the site of a previous injection.

An 8 mm 31G insulin syringe (BD, Franklin Lakes, NJ, USA) was used for intratumoral injections. NNPs and BNPs were vortexed and sonicated using a Vibra Cell sonicator (Sonics & Materials, Inc.; Danbury, CT, USA) for 30 s before use. Mice were anesthetized prior to the procedure. The needle was inserted intratumorally such that the tip was positioned in the center of the tumor, and 50 µl of drug was slowly injected over approximately 15 seconds. The needle was then held in this position for 10 seconds and slowly withdrawn to minimize backflow. Gentle pressure was applied to the site of injection to prevent leakage.

Statistical analysis

Statistical analyses were conducted using Microsoft Excel 2016 for Mac (Microsoft, Redmond, WA, USA) and Prism 7 (GraphPad, La Jolla, CA, USA). Statistical significance between experimental groups was determined using two-tailed Student's t-tests for two-sample, equal variance datasets, with significance at $p < 0.05$. Statistical significance between flow cytometry populations was

determined by FlowJo (FlowJo LLC) using the Kolmogorov-Smirnov (K-S) algorithm. The K-S algorithm is used to determine the confidence interval with which it can be asserted that two univariate histograms are different.[90,91] Notably, for analysis of flow cytometry data, this method is most ideal for smaller populations; with larger populations, there may be mathematical significance in situations where there may not be biological significance.

Division of labor

Julia Lewis, PhD, and Patrick Monico performed all animal breeding and genotyping. Hee-Won Suh, PhD, conducted polymer synthesis, nanoparticle synthesis, and nanoparticle loading. NNP to BNP conversion was performed by Emily Yin and Hee-Won Suh. Cell culture and cell viability experiments were conducted by Emily Yin. Mouse injections and tumor measurements were performed by Emily Yin and Alison Lee. Frozen tissue section preparation and confocal microscopy were performed by Emily Yin. Formalin-fixed tissue was paraffin embedded, sectioned and stained with H&E by the Yale Dermatopathology Lab. Flow cytometry was performed by Emily Yin and Julia Lewis.

RESULTS

NP uptake by PDV cells in vitro

In order to assess NP association with SCC cells *in vitro,* we incubated cells with fluorescent-dye loaded NNP or BNP and quantified fluorescence of cells by flow cytometry. DiD/BNP had enhanced association with PDV SCC cells compared with DiD/NNP *in vitro* (**Figure 4**). This relationship was consistent at both 6 and 24 hours and at higher (1 mg/ml) and lower (0.1 mg/ml) NP concentrations. A comparison of averaged median fluorescence intensities (MFI) is also shown in **Figure 4**, in which ΔMFI represents the change in MFI between 6 and 24 hours. **Table 1** displays p-value results for Student's T-tests comparing MFIs from each of the samples. Greater fluorescence was observed in samples incubated with 1 mg/ml DiD/NNP and DiD/BNP compared with their respective 0.1 mg/ml samples. There was enhanced association of both DiD/NNP and DiD/BNP with cells at 24 hours compared with 6 hours (**Figure 4C**).

Next, we sought to determine whether the association was due to NP adhesion to the cell surface or whether NPs were being internalized by cells. By confocal imaging, greater fluorescence in DiD/BNP-treated samples compared to DiD/NNP-treated samples was consistently observed (**Figure 5**). When the Ep-CAM cell surface marker stain was used, DiD fluorescence was observed co-localizing with the surface stain in some areas and was also distributed inside the cell membrane (**Figure 5B-C**), suggesting that NPs both adhere to the cell surface and are internalized by cells.

Figure 4. Bioadhesive nanoparticles (BNP) showed superior association with PDV squamous cell carcinoma cells relative to non-bioadhesive nanoparticles (NNP). Cells were harvested and analyzed by flow cytometry at (A) 6 hours and (B) 24 hours after co-incubation with 0.1 mg/mL or 1 mg/mL fluorescent dye-loaded NNP or BNP.

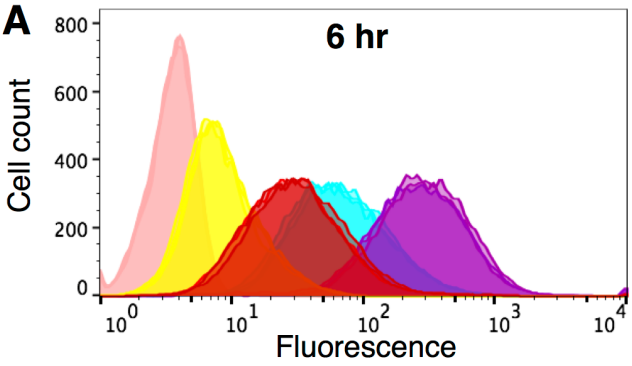

Sample	MFI (Mean ± SD)
Control	3.68 ± 0.02
0.1 mg/ml NNP	7.96 ± 0.39
0.1 mg/ml BNP	29.93 ± 2.05
1.0 mg/ml NNP	62.67 ± 3.90
1.0 mg/ml BNP	269.00 ± 19.00

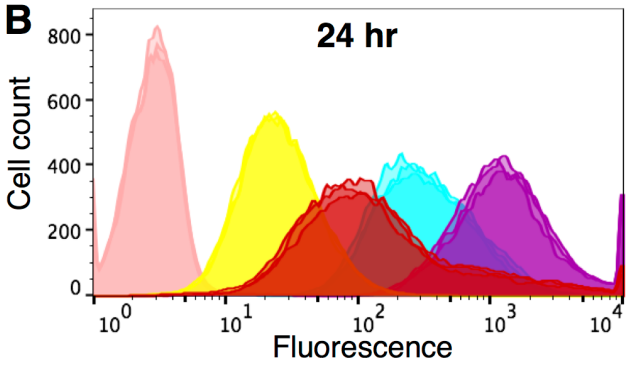

Sample	MFI (Mean ± SD)	ΔMFI (MFI_{24hr} – MFI_{6hr})
Control	2.87 ± 0.04	-0.81
0.1 mg/ml NNP	24.37 ± 0.25	16.40
0.1 mg/ml BNP	111.33 ± 10.97	81.40
1.0 mg/ml NNP	295.00 ± 24.88	232.33
1.0 mg/ml BNP	1196.00 ± 88.61	927.00

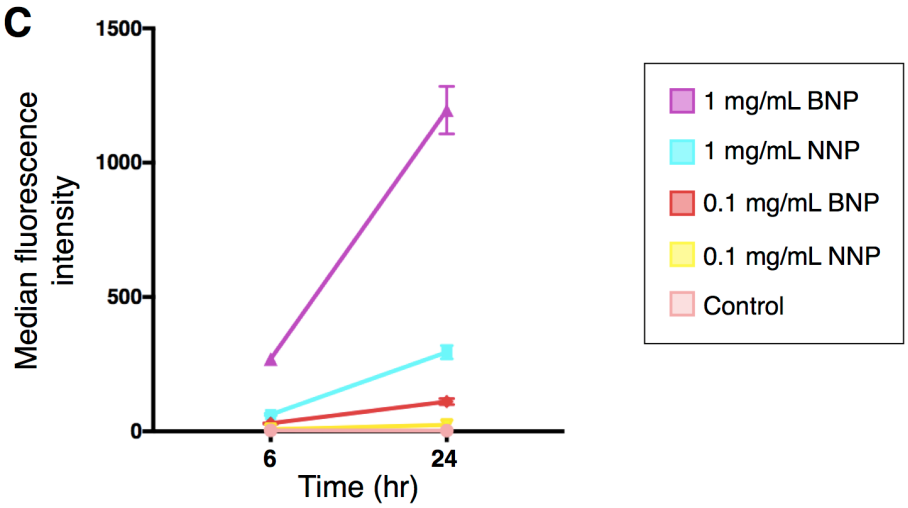

Table 1. Results of Student's T-test (two-tailed, two-sample equal variance) indicates increased association of BNP compared to NNP with cells at both time points, and increased association of dye particles at 24 hours compared with 6 hours for both NNP and BNP samples. (A) Comparison of non-bioadhesive nanoparticles (NNP) and bioadhesive nanoparticles (BNP) samples at each combination of time-point and concentration. (B) Comparison of 6-hour and 24-hour samples for NNP and BNP at each concentration.

(A)

Time-point	**NP Concentration**	**NNP vs. BNP P-value**
6 hours	1 mg/ml	0.000051
6 hours	0.1 mg/ml	0.000053
24 hours	1 mg/ml	0.000071
24 hours	0.1 mg/ml	0.000163

(B)

Sample	**NP Concentration**	**6 hr vs. 24 hr P-value**
NNP	1 mg/ml	0.000090
NNP	0.1mg/ml	<0.0000001
BNP	1 mg/ml	0.000060
BNP	0.1mg/ml	0.000226

Figure 5. Confocal microscopy shows particle-encapsulated fluorescent dye (red) inside PDV squamous cell carcinoma cells after 24-hour culture. (A) Control, DiD/NNP, and DiD/BNP samples displayed as stacked images. (B) Image montage shows cross-sections at 0.5 μm intervals through the thickness of the cells. (C) Cells at higher power show dye-loaded NNP observed both inside the cell and on the surface (co-localizing with Ep-CAM).

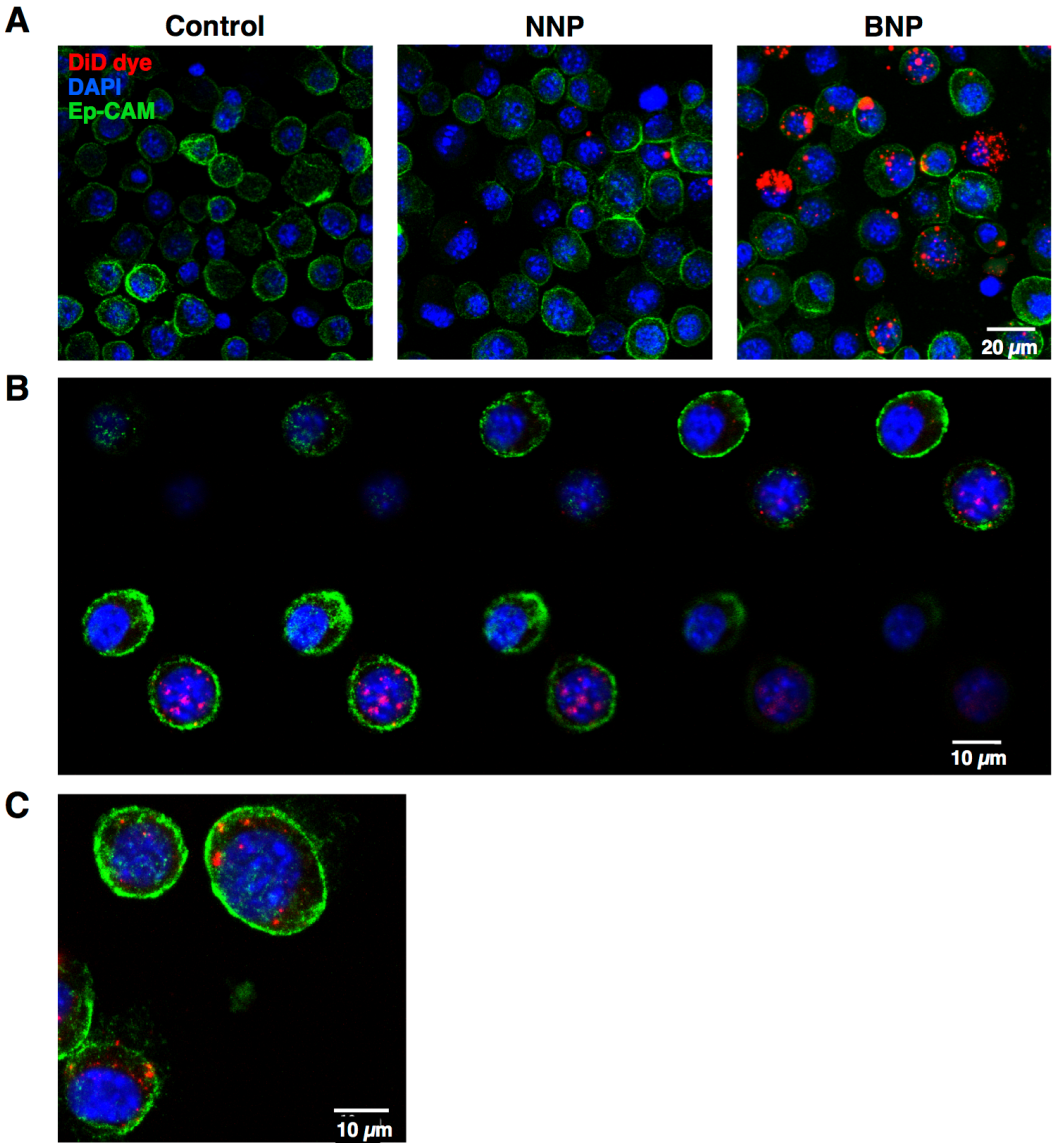

Analysis of DiD/NNP distribution in cells after topical application

To determine the distribution of NPs after topical application, we applied DiD/NNP to the shaved skin of mice and assessed skin by confocal microscopy. While BNPs would be expected to remain on the surface due to their bioadhesive properties, we hypothesized that NNPs would absorb into the skin and therefore be a better mode of chemotherapeutic drug delivery. DiD/NNP suspended in 5% di(ethylene glycol) ethyl ether was applied topically to shaved skin on the flanks of mice and occluded with a band-aid in order to visually assess the dispersion of NPs after topical application. With the goal of maximizing nanoparticle penetration through the epidermis, di(ethylene glycol) ethyl ether was selected as a solvent, as it is commonly used to increase epidermal drug penetration. Frozen sections were assessed qualitatively by confocal microscopy (**Figure 6**).

The distribution of DiD/NNP after topical application was further assessed by flow cytometry of harvested skin cells (**Figure 7**). Langerhans cells were gated on CD45+, MHC II+, and CD3-; T-cells were gated on CD45+, CD3+, and MHC II- (**Supplemental Figure S1**). There was an increased association of DiD/NNP with Langerhans cells in the epidermis compared to DiD alone and control (K-S >99.9%) (**Figure 7A)**. Similarly, there was an enhanced association of DiD/NNP with T-cells in the epidermis (K-S >99.9%) (**Figure 7B**). CD45- cells from the epidermis (**Figure 7C**), largely representing keratinocytes, also showed improved association with DiD/NNP (K-S >99.9%), as did CD45- cells from the dermis (K-S >99.9%) (**Figure 7D**). The T(X) values indicate that in each subset of cells, the DiD/NNP and control populations were statistically different.

Figure 6. Confocal microscopy shows accumulation of dye-loaded non-bioadhesive nanoparticles (red) suspended in 5% di(ethylene glycol) ethyl ether in the epidermis and hair follicles. Nuclei are stained with DAPI (blue). (A) Control (no topical application). (B) 4 hours after topical application; higher power at right. (C) 72 hours after topical application; higher power at right.

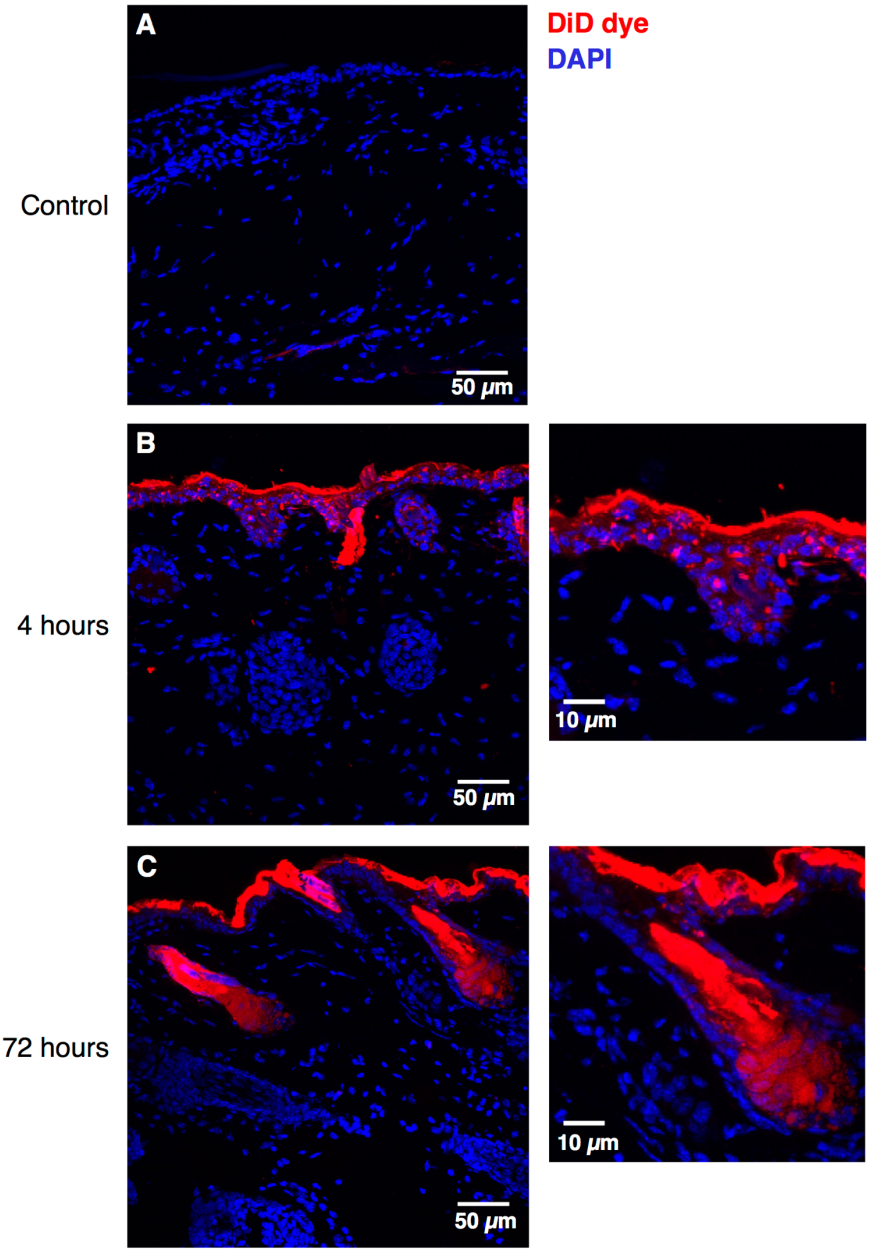

Figure 7. Topical application of DiD dye-loaded non-bioadhesive nanoparticles (NNPs) on the skin of mice results in enhanced association of dye with epidermal, dermal, and local immune cells compared to DiD application alone. Fluorescence of PDV squamous cell carcinoma cells was measured by flow cytometry 72 hours after topical skin application of DiD or DiD/NNP. (A) Langerhans cells (CD45+ MHC II+ CD3-) in the epidermis. (B) T-cells (CD45+ CD3+ MHC II-) in the epidermis. (C) CD45- cells in the epidermis. (D) CD45- cells in the dermis**.** Each plotted curve represents data from one mouse. Control populations represent mice that received injections of an equal volume of 1x PBS. Median fluorescence intensity (MFI) for each sample is shown in the corresponding tables. ΔMFI refers to the change in MFI between each sample and the control.

A

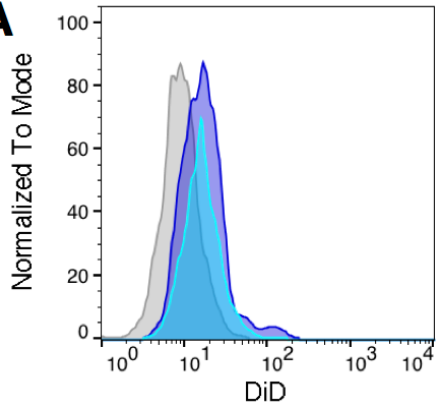

Sample	MFI	ΔMFI
Control	9.06	--
DiD	16.1	7.04
DiD/NNPs	16.3	7.24

B

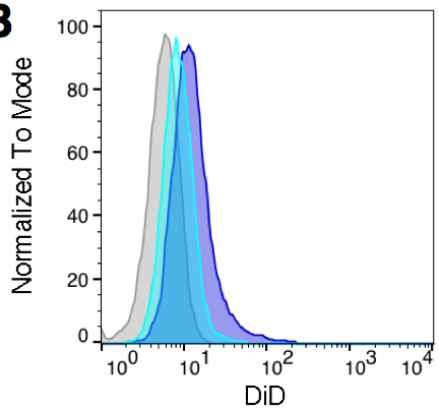

Sample	MFI	ΔMFI
Control	5.80	--
DiD	8.41	2.62
DiD/NNPs	11.9	6.1

C

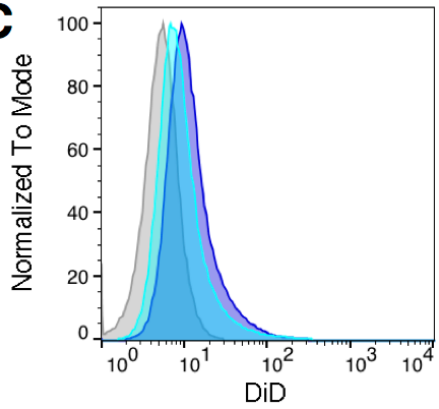

Sample	MFI	ΔMFI
Control	5.35	--
DiD	8.20	2.85
DiD/NNPs	10.6	5.25

D

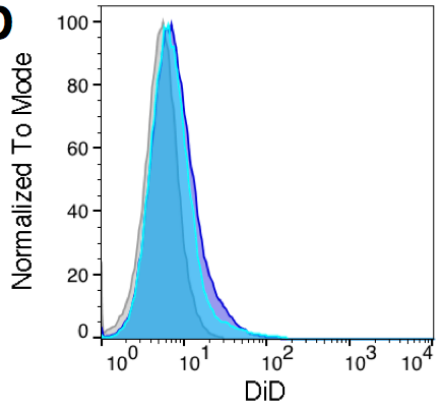

Sample	MFI	ΔMFI
Control	5.35	--
DiD	6.78	1.43
DiD/NNPs	7.28	1.93

Distribution of DiD/BNP after intratumoral injection

To assess the distribution of BNPs after intratumoral injection, we injected 100 µl of DiD/BNP into established PDV tumors at 4 weeks after tumor transplantation. We harvested the tumors after 72 hours and digested the tissue for analysis of fluorescence by flow cytometry. We also harvested the draining inguinal lymph node to address the potential for targeting immune cells. Gating of defined cell populations is shown in **Supplemental Figure S1.** Flow cytometry demonstrated significant association of DiD/BNP with a variety of cell types harvested from the draining lymph node, tumor, and skin (**Figure 8**). Comparing CD45- tumor cells, the treated samples were significantly different from the control (K-S >99.9%). The subset of CD45+ cells from the tumor was also assessed to determine the association of particles with local, tumor-associated immune cells, with increased fluorescence seen in the treated sample (K-S >99.9%). There was also a difference between treated and untreated samples of CD45+ cells from the draining lymph nodes (K-S >99.9%).

To visualize the anatomical distribution of NPs after intratumoral injections, DiD/BNP injections were repeated on another tumor for analysis by confocal microscopy. Imaging of frozen sections of these tumors showed fluorescent dye throughout the tumor, indicating tumor-wide penetrance of the intratumoral injection (**Figure 9**).

Figure 8. At 72 hours after intratumoral injection of 100 µL fluorescent dye-loaded bioadhesive nanoparticles, there was significant association of nanoparticles with cells harvested from the tumor and draining lymph node as assessed by fluorescence on flow cytometry. (A) CD45- cells from tumor. (B) CD45+ cells from tumor. (C) CD45+ cells from lymph node.

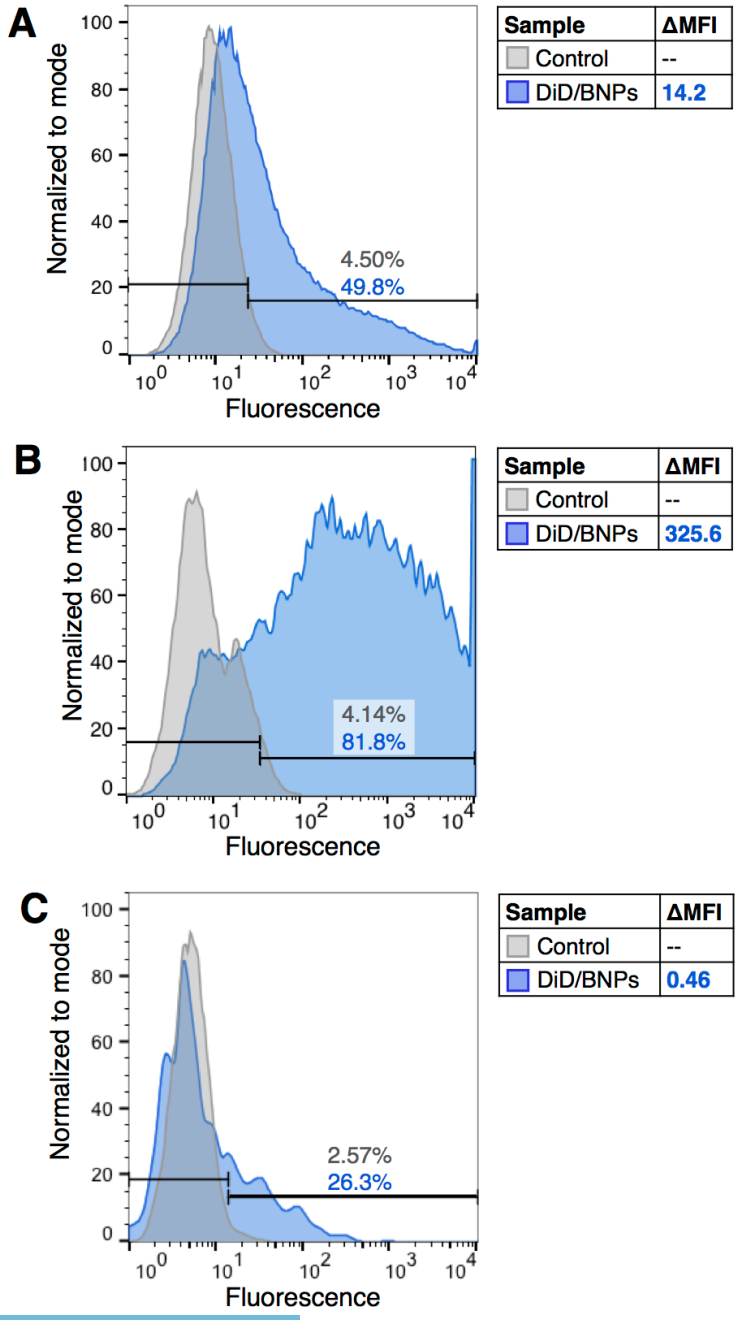

Figure 9. After intratumoral injection of 100 µl of fluorescent dye-loaded bioadhesive nanoparticles, nanoparticles were visualized by confocal to be distributed throughout the tumor. Concentration of nanoparticles within injected tumors was variable. (A) Nanoparticles were observed dispersed throughout the imaged area of a tumor. (B) Images from another injected tumor show nanoparticle dispersion throughout the layers of the skin and tumor, from minimal dye visibility in the epidermis (top) to the highly saturated tumor (bottom).

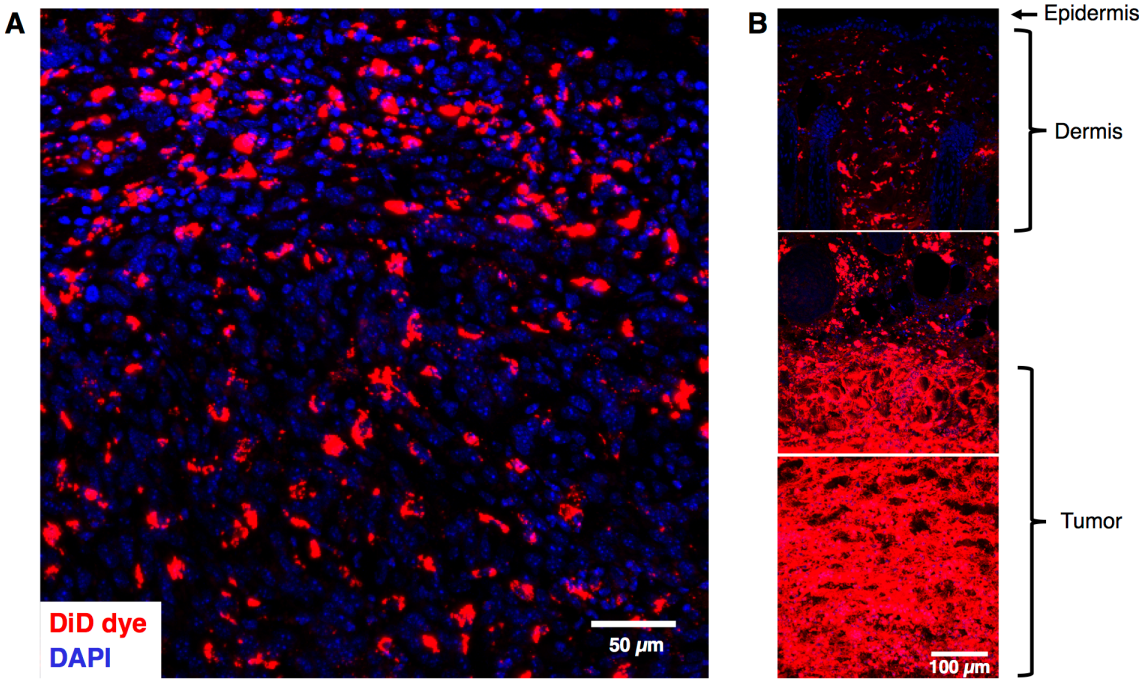

Cytotoxicity of CPT, CPT/NNP, and CPT/BNP in vitro

To compare the cytotoxic efficacy of our delivery methods *in vitro*, we used the CellTiter-Glo® Luminescent Cell Viability Assay (Promega) to measure cell viability after treatment of PDV cells with CPT, CPT/NNP, or CPT/BNP. Cytotoxicity assays were conducted at 24, 48, and 72 hours of incubation with the drug (**Figure 10**). At these time points and the selected range of concentrations, the viability curve of paclitaxel was not well visualized. NP encapsulation was attempted for each drug. However, only CPT was successfully encapsulated in PLA-HPG, and therefore this drug was used for subsequent experiments.

The time-point selected for further study was 48 hours, due to the ability to visualize the full viability curve of CPT at this time. To compare NP-encapsulated drug with drug alone, cells were incubated with CPT, CPT/NNP, or CPT/BNP for 48 hr. The three treatments had similar effects on cell viability (CPT IC_{50}=0.2770 [95% CI: 0.2365, 0.3246]; CPT/NNP IC_{50}=0.4283 [0.3387, 0.5423]; CPT/BNP IC_{50}=0.1708 [0.1444,0.2020] (**Figure 11**). Although statistically different, it is not clear from this experiment whether the difference has biological or clinical significance.

Figure 10. PDV cells were incubated with paclitaxel or camptothecin to assess the cytotoxicity and IC_{50} of each drug. Cell viability was measured by CellTiter-Glo® Luminescent Cell Viability Assay (Promega) at (A) 24, (B) 48, and (C) 72 hours.

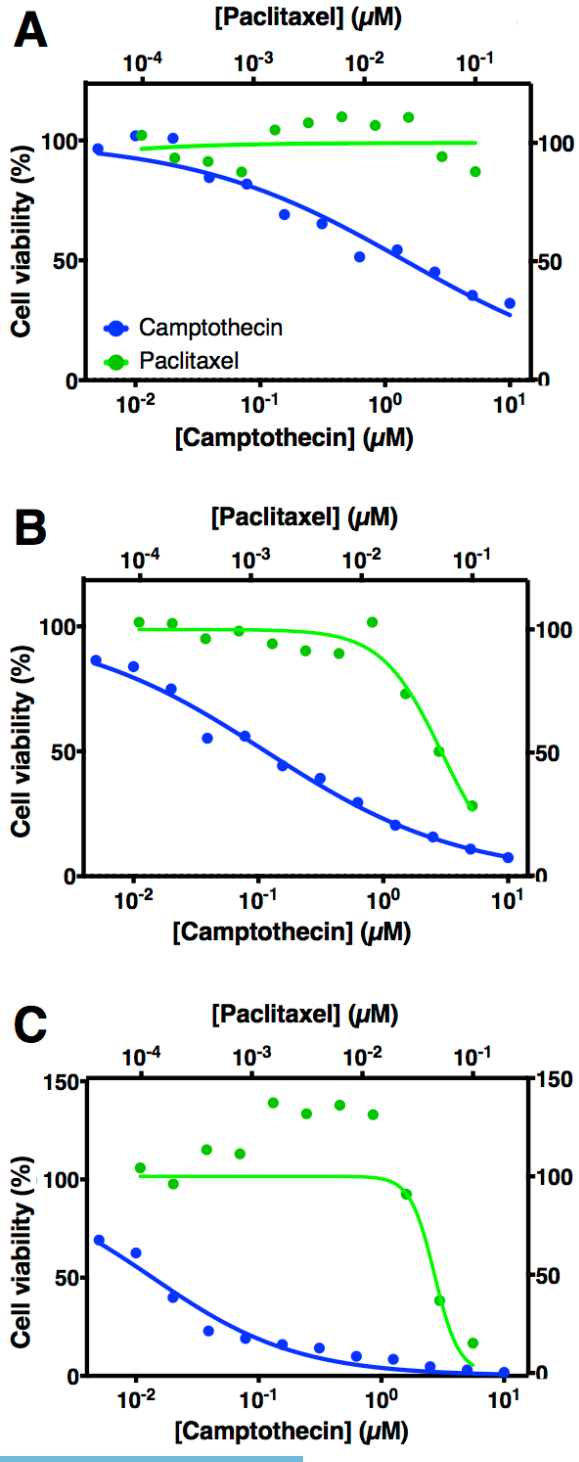

Figure 11. Incubation of PDV cells with camptothecin-loaded non-adhesive nanoparticles (CPT/NNP) resulted in slightly increased cell death at 48 hours compared to incubation with camptothecin (CPT) or CPT-loaded bioadhesive nanoparticles (CPT/BNP). Cell viability was measured by the CellTiter-Glo® Luminescent Cell Viability Assay (Promega). The three treatments had statistically different IC_{50} values: CPT IC_{50}=0.2770 [95% CI: 0.2365, 0.3246], CPT/NNP IC_{50}=0.4283 [0.3387, 0.5423], CPT/BNP IC_{50}=0.1708 [0.1444,0.2020].

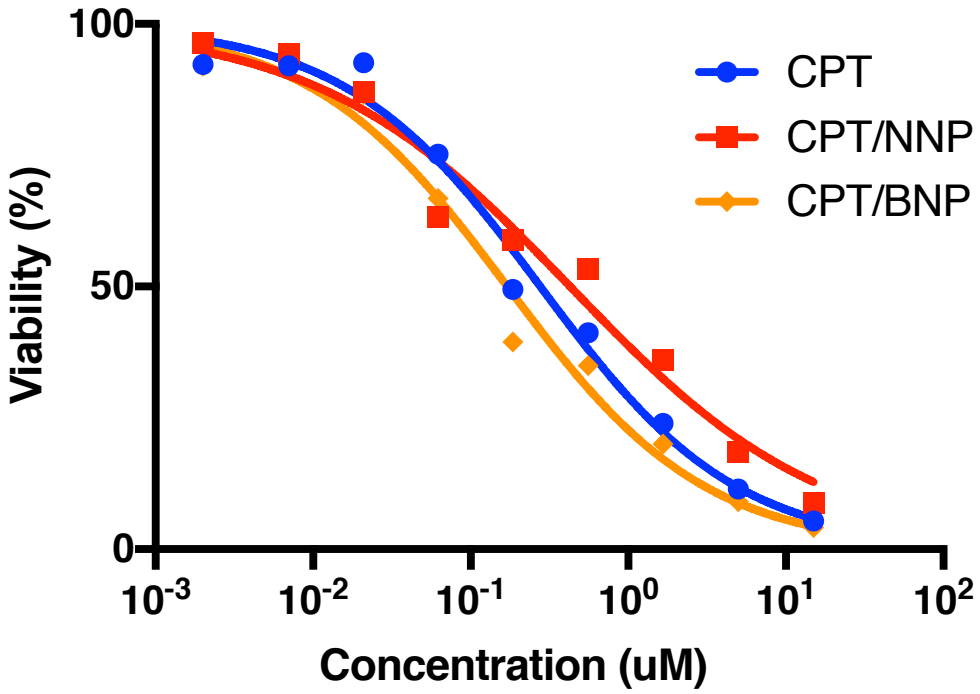

Efficacy of CPT, CPT/NNP, and CPT/BNP in treating PDV SCC tumors

In a small pilot study (n=4), mice with established PDV tumors were treated with intratumoral injections of CPT/BNP or 1x PBS to determine the efficacy of CPT/BNP *in vivo.* Control mice treated with 1x PBS injections showed significant, rapid tumor growth over 4 weeks of observation, while complete resolution of the transplanted tumor was seen in all CPT/BNP treated mice (n=2) (**Figure 12**). Tumors were harvested and fixed in 4% PFA for sectioning, and sections were stained with H&E. Large tumors were confirmed by histology in both of the control mice (**Figure 12C**), while no tumors were observed by histological examination in the two CPT/BNP-treated mice (**Figure 12D**).

Given concern for potential systemic toxicity, we used a lower dose of CPT and increased frequency of treatments in our subsequent study. We also compared CPT/BNPs to CPT in an intralipid 20% vehicle (CPT/IL) and CPT/NNPs. The dose of CPT was reduced from 0.500 mg to 0.125 mg per injection, while the frequency of injections increased from weekly to twice per week. This study (n=25) showed efficacy of all three CPT-containing treatment groups. **Figure 13** shows the Kaplan-Meier survival analysis for each group, in which the endpoint represents the tumor reaching a diameter greater than or equal to 1.0 cm in any direction. Each of the three CPT-containing samples (CPT/IL, CPT/NNP, CPT/BNP) was significantly different compared to the IL-only control (p=0.013, 0.002, 0.002, respectively). There was no statistical difference in the Kaplan-Meier survival analyses among CPT/IL, CPT/NNP, and CPT/BNP ($p_{(CPT/IL\ v.\ CPT/NNP)} = 0.1259$; $p_{(CPT/IL\ v.\ CPT/BNP)} = 0.1744$; $p_{(CPT/NNP\ v.\ CPT/BNP)} =$

0.9091). However, there was a trend toward significance in comparing CPT/NNP and CPT/BNP samples with CPT/IL, suggesting that CPT/NNP and CPT/BNP may have enhanced antitumor effects. In addition, examination of the histology of the tumors suggested that external tumor measurements in the CPT/NNP and CPT/BNP groups may over-estimate the actual tumor burden due to increased necrosis compared to CPT/IL-treated mice.

Figure 12. In a pilot study of mice with transplanted PDV tumors (N=4), tumors were treated with two weekly intratumoral injections of 0.5 mg/100 µl camptothecin bioadhesive nanoparticles (CPT/BNP) or 1x PBS (control). While control mice showed rapid tumor growth over the 3 weeks after initiation of treatment (A, C), tumors treated with CPT/BNP had complete resolution of their tumors (B, D). Images are from 10 days after final injection.

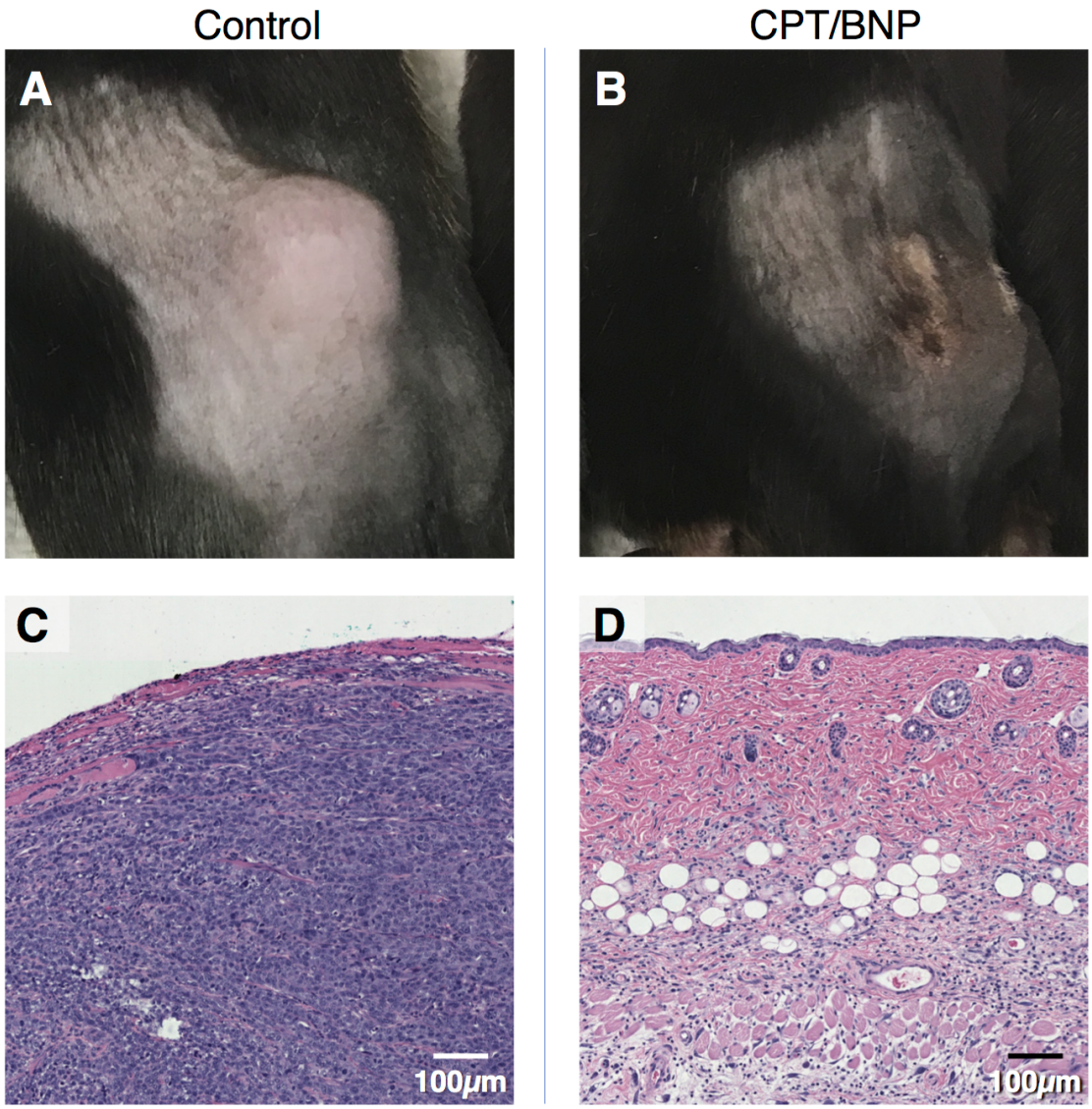

Figure 13. Kaplan-Meier survival analysis indicated a significant difference in time to 1 cm between the intralipid 20% (IL) control and each of the CPT groups: CPT in IL (CPT/IL), CPT/NNP, and CPT/BNP (N=20). Survival of CPT/IL (p=0.013), CPT/NNP (p=0.002), CPT/BNP (p=0.002) were significantly different compared to the control. No significant difference was observed between the three CPT treatment groups ($p_{(CPT/IL\ v.\ CPT/NNP)} = 0.1259$; $p_{(CPT/IL\ v.\ CPT/BNP)} = 0.1744$; $p_{(CPT/NNP\ v.\ CPT/BNP)} = 0.9091$). Mice received twice weekly intratumoral injections containing 0.125 mg CPT in a 50 µl volume. A treatment was skipped if either of the following were true: (1) ulceration at the site of injection, or (2) tumor was neither visible nor palpable.

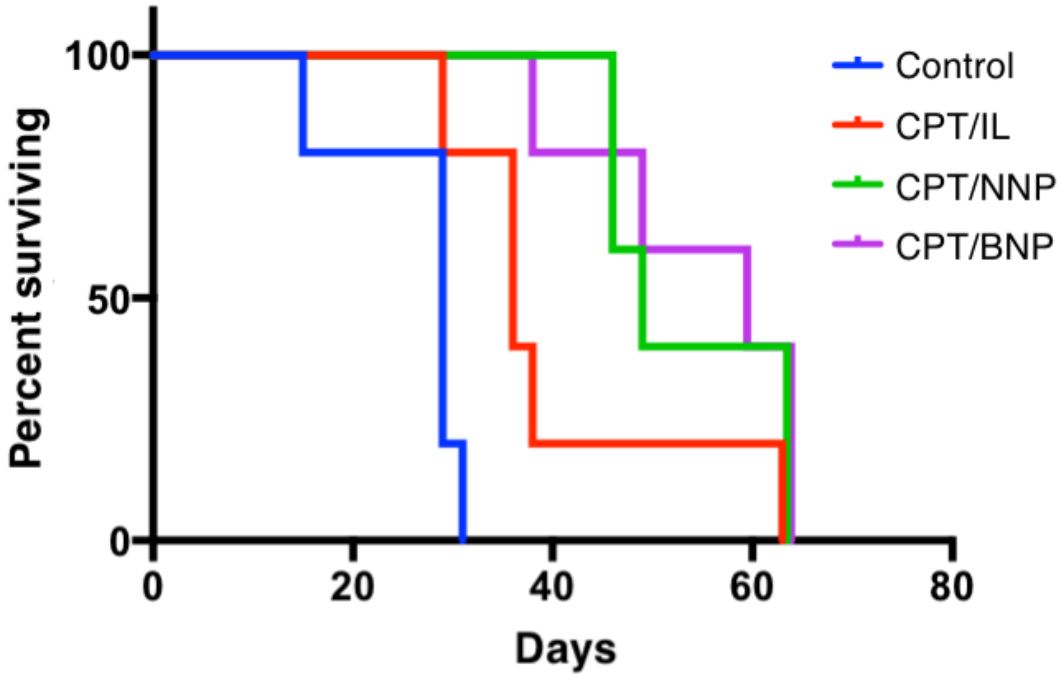

DISCUSSION

Polymer NPs can be employed as an effective drug delivery system and may be particularly well-suited for the treatment of malignant tumors. Given the limitations of current treatments in skin cancer, NPs provide a delivery method for chemotherapeutic agents that may improve treatment efficacy and decrease the risk of tumor recurrence. This is the first study to assess the efficacy of NP-encapsulated chemotherapeutic agents in the treatment of skin cancer. Our preliminary results demonstrate the efficacy of PLA-HPG NPs in the delivery of CPT for the treatment of SCC in mice.

As we had hypothesized based on prior studies, BNPs showed an increased association with PDV cells compared with NNPs. This can be explained by the aldehyde-rich surface chemistries of BNPs, which facilitate covalent bonding to cellular proteins. We not only observed the association of dye-loaded NPs with cells, but also confirmed internalization of NPs by PDV cells via confocal microscopy. The latter further suggested that NPs, in particular BNPs, may be effective at directly targeting malignant cells. While a specific mechanism of uptake has not been described for PLA-HPG NPs, prior studies suggest that a number of different pathways may be at work. For instance, PLA-PEG NPs have been shown to be taken up by receptor-mediated endocytosis.[92] Macropinocytosis has also been implicated as a pathway of internalization for other classes of NPs.[93] The predominant method of uptake may also depend on cell type and local environment.

Our observation of significant fluorescence in both NNP- and BNP- treated samples at 6 hours suggests that an NP-based delivery method could rapidly begin targeting tumor cells within hours. The increased association at 24 hours also provides evidence of the continued capacity of PDV cells to associate with NPs with prolonged co-incubations and lends support to the depot effect advantage of NPs. Additional studies at longer time-points may help determine when and at what concentration a plateau in NP association with cells is reached. This may help determine the ideal concentration of NP for therapeutic use in order to maximize treatment efficacy.

We also found that after topical application of NNPs, there was significant penetration of particles through the full thickness of the epidermis as well as in hair follicles, by as early as 4 hours and persisting for at least 72 hours. There was enhanced uptake of NNPs by cells compared to fluorescent dye alone, including in keratinocytes in the epidermis, fibroblasts in the dermis, and T-cells and Langerhans cells in the epidermis. This supports the use of NNPs as a topical delivery method and also suggests NPs may be an effective delivery system for immune-modulating therapies. Notably, the K-S algorithm was used to determine whether there were statistical differences in fluorescence between these populations of cells. While this statistic is recommended for comparing populations, it is notably a measure of mathematical and not biological difference. As the value of *n* increases, particularly in our flow cytometry data that has populations in the thousands to hundreds of thousands, there is an increasing likelihood of a >99% difference between two populations. As such,

while we can conclude that there is a true difference in the association of DiD/NNPs and DiD alone with T-cells, Langerhans cells, epidermal keratinocytes, and connective tissue cells in the dermis, the biological or clinical significance of these findings is more subjective. However, we can compare the relative impact of NNP delivery on various cell types by comparing the ΔMFI of various cell types. For instance, Langerhans cells (ΔMFI=7.24), T-cells (ΔMFI=6.1), and epidermal keratinocytes (ΔMFI=5.25) have greater uptake of NNPs compared to dermal fibroblasts (ΔMFI=1.93).

Despite the difference in surface chemistry between NNPs and BNPs, and the related difference in cell association, there was only a small difference in effect on cell viability among CPT/NNP, CPT/BNP, and CPT *in vitro*. CPT/NNP had the lowest IC_{50}, while CPT/BNP had the highest IC_{50}, and thus a higher concentration of CPT/BNP would be necessary to achieve the same degree of cytotoxicity. This may appear contrary to our previous findings that BNPs have preferable association with PDV cells compared to NNPs; however, association with NPs is not necessary for the drug to exert its cytotoxic effects, as free-floating NPs will continue to release active CPT. In addition, while these results were statistically different, their clinical significance is less clear. Taken together, these findings may also suggest that the lack of cytotoxic advantage of CPT/BNP compared to CPT/NNP is not related to the degree of NP-cell kinetics, but rather may be explained by drug-cell or drug-NP kinetics. Previous studies using CPT in PLA-HPG nanoparticles have shown that at room temperature in buffered water, the particles release slightly over half of their contents within 24 hours, and the

remaining encapsulated drug is released over a period of 1 week.[60] However, this release profile may not be applicable for *in vitro* studies in buffered cell media at 37ºC. Drug may be released more quickly in these conditions, thereby minimizing the advantages conferred by NP encapsulation. While less likely, it is also possible that the nanoparticles may degrade and release CPT more slowly in these settings, such that an incubation time longer than 48 hours would be necessary to observe differences between NNPs and BNPs. Previous studies from our research group have suggested that a difference in antitumor efficacy between delivery methods may be observed only in *in vivo* studies, while no difference is observed *in vitro*. Deng et al. showed that PLA-HPG CPT/NNP significantly decreased tumor burden in Lewis lung carcinoma-bearing mice compared to PLA-PEG CPT/NNP, however no difference in cytotoxic efficacy was seen between the PLA-HPG and PLA-PEG CPT/NNP *in vitro.*[60]

Our initial *in vivo* pilot study also demonstrated the efficacy of CPT/BNP in the treatment of established SCC tumors. Due to concern for potential systemic toxicity associated with such a high dose of CPT, we used a decreased dose and increased frequency of treatments in our subsequent study. In this second experiment, several mice received fewer than the scheduled biweekly doses, as injections were not administered if the mice had ulceration from prior injections or in the absence of a visible or palpable tumor. Given the absence of complete resolution in the tumors in this experiment, a higher dose of CPT is likely necessary to definitively treat these tumors.

Furthermore, our study demonstrated that CPT/NNP and CPT/BNP may be more effective in the treatment of established PDV SCC tumors compared to CPT/IL. In our Kaplan-Meier analysis, there was a trend towards superiority of CPT/NNP and CPT/BNP compared to CPT/IL ($p_{(CPT/IL\ v.\ CPT/NNP)} = 0.1259$; $p_{(CPT/IL\ v.\ CPT/BNP)} = 0.1744$). We had hypothesized that both NNPs and BNPs would have superior antitumor efficacy compared to drug alone. As previously described, polymer NPs are notable for the advantages of gradual release and producing a depot effect, as well as advantages secondary to the EPR effect. Thus, the lack of statistical difference between NP-encapsulated drug and drug alone may suggest an insufficient sample size, or it may point to these NP advantages having been minimized or hindered by another process. As previously proposed, immediate release of drug from the particles after intratumoral injection may decrease advantages in efficacy expected from controlled-release. Injection of a relatively large volume of drug into the tight space of the tumor interstitium may cause structural changes to the tissue, vasculature, or lymphatic drainage that minimize the EPR effect which gives NPs their antitumor advantage.

In addition, we had hypothesized that CPT/BNP would have superior efficacy compared to CPT/NNP due to BNPs' enhanced ability to bind to cellular proteins and increased uptake *in vivo*. This pattern was seen in prior studies of glioblastoma and intraperitoneal uterine serous carcinoma from our group. However, in glioblastoma, the continual flow of CSF through the brain may make NNPs easily cleared away, while in the case of intraperitoneal carcinomas, intraperitoneal fluid is also absorbed and replenished over time. Relative to these

tumor models, there is likely relatively limited drainage from the self-contained PDV SCC tumors. As described in the EPR effect, lymphatics in tumors have poor drainage, and in such a setting, NNPs and BNPs may be similarly retained in the tumor interstitum. Future studies may employ dye-loaded NPs to compare the degree to which NNPs and BNPs track to the draining lymph nodes. While we believe that NP delivery has advantages that can be exploited to improve the treatment of cutaneous malignancies, our preliminary data has not been able to definitively confirm this hypothesis.

Our study has a few limitations. First, when visualizing dye by confocal microscopy, we cannot be certain that we are visualizing only NPs and not free dye that has been released from NPs. Similarly, we know that drug release from NPs is dependent on the encapsulated drug, therefore the behavior of dye-loaded NPs may not be highly predictive of CPT-loaded NPs. Another limitation is the potential for human bias or variation in our procedures. Our studies were not blinded, as they were in large part conducted by a single researcher in an effort to minimize researcher-to-researcher variation in injection and measurement techniques. When injecting tumors that may range significantly in size, shape, and density, it is impossible to fully standardize injection techniques. However, we sought to replicate our injection technique as precisely as possible from mouse to mouse. Finally, the external measurement of tumors may be complicated by inflammation and necrosis that occurs secondary to treatment. Histological examination of tumors suggested that tumor burden may be over-estimated in NNP-treated and BNP-treated mice due to widespread necrosis.

Additional studies are underway to optimize the concentration and frequency of drug delivery in order to consistently and definitively treat tumors. Future experiments will also aim to assess other potential injection techniques to determine the most effective means of delivering our treatment. Other chemotherapeutic drugs will be tested, as they may offer increased efficacy for our tumor model. While paclitaxel was difficult to encapsulate in PLA-HPG NPs, other types of polymers may be better suited for encapsulating the drug. Epithilone B has also been found effective in a number of other murine studies, including in uterine serious carcinoma, and has been encapsulated in PLA-HPG.[79] While our current tumor model employs subcutaneous tumors, we may also study NP efficacy in other tumor models, such as chemically induced tumors via topical application of DMBA and TPA. For these models, cutaneous application of treatments may be used in conjunction with other delivery methods, such as microneedles, ultrasound, or tape-stripping.[94]

Aside from directly targeting malignant tumor cells, the local immune system may also be an effective target for antitumor therapies. Our study found significant NP uptake both in Langerhans cells and T-cells in the local tumor environment, as well as in cells in the draining lymph node. Immune-stimulating drugs, such as imiquimod or interferons, may therefore be effectively delivered by NP encapsulation. Imiquimod is currently used as a topical therapy to stimulate the local immune system to attack tumor cells; encapsulation in NPs may prolong and enhance the effects of the drug. Additionally, co-encapsulation

simultaneous administration with a chemotherapeutic drug or may produce an additive or synergistic effect.

In addition to the potential of NP delivery in the treatment of cutaneous malignancies, NP encapsulation can also enhance existing preventative skin cancer strategies. Our research group recently developed a novel, BNP-based sunblock that enhances duration of protection and minimizes the production of reactive oxygen species typically associated with chemical UVR-blocking agents.[95] These benefits are a result of BNPs engineered for minimal release of drug over time and adherence to the stratum corneum. We also plan to use our NP delivery platform to provide post-UV protection in the form of antioxidants and "triplet-state quenchers" to counteract free radicals and oxidative stress that can lead to DNA damage hours after sun exposure.[96]

In conclusion, our study demonstrates that polymer-based NPs are a promising drug delivery system for chemotherapeutic treatment of skin cancer, and that CPT/BNPs may have the capacity to definitively treat PDV SCC. While surgery will likely remain an important therapy for skin cancer, an NP-based treatment may offer an improved therapeutic option for patients with lesions affecting large surface areas or who are otherwise poor candidates for surgical therapy. NP delivery may also allow post-surgical treatment in the surgical bed to prevent recurrence and eliminate any remaining cancer cells. Through these methods, NP encapsulation may enhance the prevention and treatment of skin cancer, offering superior efficacy when compared to existing preventative and therapeutic methods.

REFERENCES

1. Rogers HW, Weinstock MA, Feldman SR, Coldiron BM. Incidence estimate of nonmelanoma skin cancer (keratinocyte carcinomas) in the US population, 2012. *JAMA Dermatology*. 2015;151(10):1081-1086.
2. Siegel RL, Miller KD, Jemal A. Cancer Statistics, 2017. *CA Cancer J Clin*. 2017;67:7-30.
3. American Cancer Society. Cancer Facts and Figures 2017. Genes and Development.
4. Lomas A, Leonardi-Bee J, Bath-Hextall F. A systematic review of worldwide incidence of nonmelanoma skin cancer. *Br J Dermatol*. 2012;166(5):1069-1080.
5. Neale RE, Davis M, Pandeya N, Whiteman DC, Green AC. Basal cell carcinoma on the trunk is associated with excessive sun exposure. *J Am Acad Dermatol*. 2007;56(3):380-386.
6. Rosso S, Zanetti R, Martinez C, et al. The multicentre south European study “Helios”. II: Different sun exposure patterns in the aetiology of basal cell and squamous cell carcinomas of the skin. *Br J Cancer*. 1996;73(11):1447-1454.
7. English DR, Armstrong BK, Kricker A, Fleming C. Sunlight and cancer. *Cancer Causes Control*. 1997;8(3):271-283.
8. Harwood CA, Surentheran T, McGregor JM, et al. Human papillomavirus infection and non-melanoma skin cancer in immunosuppressed and immunocompetent individuals. *J Med Virol*. 2000;61(3):289-297.
9. Brantsch KD, Meisner C, Schönfisch B, et al. Analysis of risk factors determining prognosis of cutaneous squamous-cell carcinoma: a prospective study. *Lancet Oncol*. 2008;9(8):713-720.
10. Joseph MG, Zulueta WP, Kennedy PJ. Squamous cell carcinoma of the skin of the trunk and limbs: the incidence of metastases and their outcome. *Aust N Z J Surg*. 1992;62(9):697-701.
11. Brougham NDLS, Dennett ER, Cameron R, Tan ST. The incidence of metastasis from cutaneous squamous cell carcinoma and the impact of its risk factors. *J Surg Oncol*. 2012;106(7):811-815.
12. Cherpelis BS, Marcusen C, Lang PG. Prognostic factors for metastasis in squamous cell carcinoma of the skin. *Dermatologic Surg*. 2002;28(3):268-273.
13. Rowe DE, Carroll RJ, Day CL. Prognostic factors for local recurrence, metastasis, and survival rates in squamous cell carcinoma of the skin, ear, and lip. Implications for treatment modality selection. *J Am Acad Dermatol*. 1992;26(6):976-990.
14. Glogau RG. The risk of progression to invasive disease. *J Am Acad Dermatol*. 2000;42(1 Pt 2):23-24.
15. Pomerantz H, Hogan D, Eilers D, et al. Long-term efficacy of topical fluorouracil cream, 5%, for treating actinic keratosis. *JAMA Dermatology*. 2015;151(9):952.
16. Gupta AK, Paquet M, Villanueva E, Brintnell W. Interventions for actinic keratoses. In: Gupta AK, ed. *Cochrane Database of Systematic Reviews*. Chichester, UK: John Wiley & Sons, Ltd; 2012.
17. Guy GP, Machlin SR, Ekwueme DU, Yabroff KR. Prevalence and costs of skin cancer treatment in the U.S., 2002-2006 and 2007-2011. *Am J Prev Med*. 2015;48(2):183-187.
18. Reeder VJ, Gustafson CJ, Mireku K, Davis SA, Feldman SR, Pearce DJ. Trends in Mohs Surgery From 1995 to 2010. *Dermatologic Surg*. 2015;41(3):397-403.
19. Swanson NA. Mohs surgery. Technique, indications, applications, and the future. *Arch Dermatol*. 1983;119(9):761-773.
20. Rogers HW, Coldiron BM. A relative value unit-based cost comparison of treatment

modalities for nonmelanoma skin cancer: Effect of the loss of the Mohs multiple surgery reduction exemption. *J Am Acad Dermatol*. 2009;61(1):96-103.

21. Christenson LJ. Incidence of Basal Cell and Squamous Cell Carcinomas in a Population Younger Than 40 Years. *J Am Med Assoc*. 2005;294(6):681.
22. Barysch MJ, Eggmann N, Beyeler M, Panizzon RG, Seifert B, Dummer R. Long-term recurrence rate of large and difficult to treat cutaneous squamous cell carcinomas after superficial radiotherapy. *Dermatology*. 2012;224(1):59-65.
23. Cognetta AB, Howard BM, Heaton HP, Stoddard ER, Hong HG, Green WH. Superficial x-ray in the treatment of basal and squamous cell carcinomas: A viable option in select patients. *J Am Acad Dermatol*. 2012;67(6):1235-1241.
24. Fitzgerald TJ, Jodoin MB, Tillman G, et al. Radiation therapy toxicity to the skin. *Dermatol Clin*. 2008;26(1):161-172.
25. Christensen SR, Leffell DJ. Cancer of the Skin. In: *Cancer: Principles and Practice of Oncology, 10th Edition*. Lippincott Williams & Wilkins; 2014.
26. Silverman MK, Kopf AW, Grin CM, Bart RS, Levenstein MJ. Recurrence rates of treated basal cell carcinomas. Part 2: Curettage-electrodesiccation. *J Dermatol Surg Oncol*. 1991;17(9):720-726.
27. Alam M, Ratner D. Cutaneous squamous-cell carcinoma. *N Engl J Med*. 2001;344(13):975-983.
28. Rowe DE, Carroll RJ, Day CL. Long-term recurrence rates in previously untreated (primary) basal cell carcinoma: implications for patient follow-up. *J Dermatol Surg Oncol*. 1989;15(3):315-328.
29. Thissen MR, Neumann MH, Schouten LJ. A systematic review of treatment modalities for primary basal cell carcinomas. *Arch Dermatol*. 1999;135(10):1177-1183.
30. Zitelli JA. Cryosurgery for skin cancer. *J Am Acad Dermatol*. 1992;26(2 Pt 1):283-284.
31. Kuflik EG, Gage AA. The five-year cure rate achieved by cryosurgery for skin cancer. *J Am Acad Dermatol*. 1991;24(6 Pt 1):1002-1004.
32. Zacarian SA. Cryosurgery of cutaneous carcinomas. An 18-year study of 3,022 patients with 4,228 carcinomas. *J Am Acad Dermatol*. 1983;9(6):947-956.
33. Fraunfelder FT, Zacarian SA, Limmer BL, Wingfield D. Cryosurgery for malignancies of the eyelid. *Ophthalmology*. 1980;87(6):461-465.
34. Gupta AK, Paquet M, Villanueva E, Brintnell W. Interventions for actinic keratoses. Gupta AK, ed. *Cochrane database Syst Rev*. 2012;12:CD004415.
35. Wolf JE, Taylor JR, Tschen E, Kang S. Topical 3.0% diclofenac in 2.5% hyaluronan gel in the treatment of actinic keratoses. *Int J Dermatol*. 2001;40(11):709-713.
36. Lebwohl M, Swanson N, Anderson LL, Melgaard A, Xu Z, Berman B. Ingenol mebutate gel for actinic keratosis. *N Engl J Med*. 2012;366(11):1010-1019.
37. Rosen RH, Gupta AK, Tyring SK. Dual mechanism of action of ingenol mebutate gel for topical treatment of actinic keratoses: Rapid lesion necrosis followed by lesion-specific immune response. *J Am Acad Dermatol*. 2012;66(3):486-493.
38. Monheit GD. Medium-depth chemical peels. *Dermatol Clin*. 2001;19(3):413-25, vii.
39. Goette DK. Topical chemotherapy with 5-fluorouracil: A review. *J Am Acad Dermatol*. 1981;4(6):633-649.
40. Salim A, Leman JA, McColl JH, Chapman R, Morton CA. Randomized comparison of photodynamic therapy with topical 5-fluorouracil in Bowen's disease. *Br J Dermatol*. 2003;148(3):539-543.
41. Grapengiesser S, Gudmundsson F, Larkö O, Ericson M, Rosén A, Wennberg AM. Pain

caused by photodynamic therapy of skin cancer. *Clin Exp Dermatol*. 2002;27(6):493-497.

42. Fink-Puches R, Soyer HP, Hofer A, Kerl H, Wolf P. Long-term follow-up and histological changes of superficial nonmelanoma skin cancers treated with topical delta-aminolevulinic acid photodynamic therapy. *Arch Dermatol*. 1998;134(July):821-826.
43. Apalla Z, Sotiriou E, Chovarda E, Lefaki I, Devliotou-Panagiotidou D, Ioannides D. Skin cancer: Preventive photodynamic therapy in patients with face and scalp cancerization. A randomized placebo-controlled study. *Br J Dermatol*. 2010;162(1):171-175.
44. Minars N, Blyumin-Karasik M. Treatment of basal cell carcinomas with pulsed dye laser: a case series. *J Skin Cancer*. 2012;2012:286480.
45. Humphreys TR, Malhotra R, Scharf MJ, Marcus SM, Starkus L, Calegari K. Treatment of superficial basal cell carcinoma and squamous cell carcinoma in situ with a high-energy pulsed carbon dioxide laser. *Arch Dermatol*. 1998;134(10):1247-1252.
46. Guterres SS, Alves MP, Pohlmann AR. Polymeric nanoparticles, nanospheres and nanocapsules, for cutaneous applications. *Drug Target Insights*. 2007;2(April):147-157.
47. Mora-Huertas CE, Fessi H, Elaissari A. Polymer-based nanocapsules for drug delivery. *Int J Pharm*. 2010;385:113-142.
48. Hobbs SK, Monsky WL, Yuan F, et al. Regulation of transport pathways in tumor vessels: Role of tumor type and microenvironment. *Proc Natl Acad Sci*. 1998;95(8):4607-4612.
49. Jain RK, Stylianopoulos T. Delivering nanomedicine to solid tumors. *Nat Rev Clin Oncol*. 2010;7(11):653-664.
50. Eblan MJ, Wang AZ. Improving chemoradiotherapy with nanoparticle therapeutics. *Transl Cancer Res*. 2013;2(4):320-329.
51. Maeda H, Wu J, Sawa T, Matsumura Y, Hori K. Tumor vascular permeability and the EPR effect in macromolecular therapeutics: A review. *J Control Release*. 2000;65(1-2):271-284.
52. Chauhan VP, Stylianopoulos T, Martin JD, et al. Normalization of tumour blood vessels improves the delivery of nanomedicines in a size-dependent manner. *Nat Nanotechnol*. 2012;7(6):383-388.
53. Noguchi Y, Wu J, Duncan R, et al. Early phase tumor accumulation of macromolecules: a great difference in clearance rate between tumor and normal tissues. *Jpn J Cancer Res*. 1998;89(3):307-314.
54. Chauhan VP, Stylianopoulos T, Boucher Y, Jain RK. Delivery of molecular and nanoscale medicine to tumors: transport barriers and strategies. *Annu Rev Chem Biomol Eng*. 2011;2(1):281-298.
55. Quintanar-Guerrero D, Allémann E, Fessi H, Doelker E. Preparation Techniques and Mechanisms of Formation of Biodegradable Nanoparticles from Preformed Polymers. *Drug Dev Ind Pharm*. 1998;24(12):1113-1128.
56. Longmire M, Choyke PL, Kobayashi H. Clearance properties of nano-sized particles and molecules as imaging agents: considerations and caveats. *Nanomedicine (Lond)*. 2008;3(5):703-717.
57. Almeida JPM, Chen AL, Foster A, Drezek R. *In vivo* biodistribution of nanoparticles. *Nanomedicine*. 2011;6(5):815-835.
58. Kocbek P, Obermajer N, Cegnar M, Kos J, Kristl J. Targeting cancer cells using PLGA nanoparticles surface modified with monoclonal antibody. *J Control Release*. 2007;120(1-2):18-26.
59. Zhao H, Li Z, Yang B, Wang J, Li Y. Synthesis of dual-functional targeting probes for cancer theranostics based on iron oxide nanoparticles coated by centipede-like polymer connected with pH-responsive anticancer drug. *J Biomater Sci Polym Ed*.

2015;26(16):1178-1189.

60. Deng Y, Saucier-Sawyer JK, Hoimes CJ, et al. The effect of hyperbranched polyglycerol coatings on drug delivery using degradable polymer nanoparticles. *Biomaterials*. 2014;35(24):6595-6602.

61. Kamaly N, Yameen B, Wu J, Farokhzad OC. Degradable Controlled-Release Polymers and Polymeric Nanoparticles: Mechanisms of Controlling Drug Release. *Chem Rev*. 2016;116(4):2602-2663.

62. Uhrich KE, Cannizzaro SM, Langer RS, Shakesheff KM. Polymeric Systems for Controlled Drug Release. *Chem Rev*. 1999;99(11):3181-3198.

63. Kainthan RK, Hester SR, Levin E, Devine D V., Brooks DE. In vitro biological evaluation of high molecular weight hyperbranched polyglycerols. *Biomaterials*. 2007;28(31):4581-4590.

64. Kainthan RK, Brooks DE. In vivo biological evaluation of high molecular weight hyperbranched polyglycerols. *Biomaterials*. 2007;28(32):4779-4787.

65. Jamshidian M, Tehrany EA, Imran M, Jacquot M, Desobry S. Poly-Lactic Acid: Production, applications, nanocomposites, and release studies. *Compr Rev Food Sci Food Saf*. 2010;9(5):552-571.

66. Pawar RP, Tekale SU, Shisodia SU, Totre JT, Domb AJ. Biomedical Applications of Poly(Lactic Acid). *PLA Appl*. 2014;4:40-51.

67. Eitenmuller J, David A, Pommer A, Muhr G. [Surgical treatment of ankle joint fractures with biodegradable screws and plates of poly-l-lactide]. *Chirurg*. 1996;67(4):413-418.

68. van der Elst M, Klein C, De Blieck-Hogervorst J, Patka P, Haarman H. Bone tissue response to biodegradable polymers used for intra medullary fracture fixation: A long-term in vivo study in sheep femora. *Biomaterials*. 1999;20(2):121-128.

69. Yeh PYJ, Kainthan RK, Zou Y, Chiao M, Kizhakkedathu JN. Self-assembled monothiol-terminated hyperbranched polyglycerols on a gold surface: A comparative study on the structure, morphology, and protein adsorption characteristics with linear poly(ethylene glycol)s. *Langmuir*. 2008;24(9):4907-4916.

70. Amoozgar Z, Yeo Y. Recent advances in stealth coating of nanoparticle drug delivery systems. *Wiley Interdiscip Rev Nanomedicine Nanobiotechnology*. 2012;4(2):219-233.

71. Song E, Gaudin A, King AR, et al. Surface chemistry governs cellular tropism of nanoparticles in the brain. *Nat Commun*. 2017;8:15322.

72. Lim WT, Tan EH, Toh CK, et al. Phase I pharmacokinetic study of a weekly liposomal paclitaxel formulation (Genexol®-PM) in patients with solid tumors. *Ann Oncol*. 2010;21(2):382-388.

73. Lee KS, Chung HC, Im SA, et al. Multicenter phase II trial of Genexol-PM, a Cremophor-free, polymeric micelle formulation of paclitaxel, in patients with metastatic breast cancer. *Breast Cancer Res Treat*. 2008;108(2):241-250.

74. Kim DW, Kim SY, Kim HK, et al. Multicenter phase II trial of Genexol-PM, a novel Cremophor-free, polymeric micelle formulation of paclitaxel, with cisplatin in patients with advanced non-small-cell lung cancer. *Ann Oncol*. 2007;18(12):2009-2014.

75. Dinndorf PA, Gootenberg J, Cohen MH, Keegan P, Pazdur R. FDA Drug Approval Summary: Pegaspargase (Oncaspar(R)) for the First-Line Treatment of Children with Acute Lymphoblastic Leukemia (ALL). *Oncologist*. 2007;12(8):991-998.

76. Molineux G. Pegylation: engineering improved biopharmaceuticals for oncology. *Pharmacotherapy*. 2003;23(8 Pt 2):3S-8S.

77. Avramis VI, Sencer S, Periclou AP, et al. A randomized comparison of native Escherichia coli asparaginase and polyethylene glycol conjugated asparaginase for treatment of

children with newly diagnosed standard-risk acute lymphoblastic leukemia: A Children's Cancer Group study. *Blood*. 2002;99(6):1986-1994.

78. Sawyer AJ, Saucier-Sawyer JK, Booth CJ, et al. Convection-enhanced delivery of camptothecin-loaded polymer nanoparticles for treatment of intracranial tumors. *Drug Deliv Transl Res*. 2011;1(1):34-42.

79. Deng Y, Yang F, Cocco E, et al. Improved i.p. drug delivery with bioadhesive nanoparticles. *Proc Natl Acad Sci*. 2016;113(41):11453-11458.

80. Caulín C, Bauluz C, Gandarillas A, Cano A, Quintanilla M. Changes in keratin expression during malignant progression of transformed mouse epidermal keratinocytes. *Exp Cell Res*. 1993;204(1):11-21.

81. Wall ME, Wani MC. Camptothecin and Taxol: Discovery to Clinic—Thirteenth Bruce F. Cain Memorial Award Lecture. *Cancer Res*. 1995;55(4):753-760.

82. Willey CD, Yang ES-H, Bonner JA. Interaction of Chemotherapy and Radiation. In: *Clinical Radiation Oncology*. ; 2016:63-79.

83. Gottlieb JA, Guarino AM, Call JB, Oliverio VT, Block JB. Preliminary pharmacologic and clinical evaluation of camptothecin sodium (NSC-100880). *Cancer Chemother Rep*. 1970;54(6):461-470.

84. Muggia FM, Creaven PJ, Hansen HH, Cohen MH, Selawry OS. Phase I clinical trial of weekly and daily treatment with camptothecin (NSC-100880): correlation with preclinical studies. *Cancer Chemother reports*. 1972;56(4):515-521.

85. Bissett D, Cassidy J, De Bono JS, et al. Phase I and pharmacokinetic (PK) study of MAG-CPT (PNU 166148): A polymeric derivative of camptothecin (CPT). *Br J Cancer*. 2004;91(1):50-55.

86. Rivory LP, Robert J. Molecular, cellular, and clinical aspects of the pharmacology of 20(S)camptothecin and its derivatives. *Pharmacol Ther*. 1995;68(2):269-296.

87. Ziomkowska B, Kruszewski S, Siuda R, Cyrankiewicz M. Deactivation rate of camptothecin determined by factor analysis of steady-state fluorescence and absorption spectra. *Opt Appl*. 2006;36(1).

88. Sunder A, Hanselmann R, Frey H, Mülhaupt R. Controlled synthesis of hyperbranched polyglycerols by ring-opening multibranching polymerization. *Macromolecules*. 1999;32(13):4240-4246.

89. Schindelin J, Arganda-Carreras I, Frise E, et al. Fiji: an open-source platform for biological-image analysis. *Nat Methods*. 2012;9(7):676-682.

90. FlowJo. Comparison Algorithms. FlowJo v10 Documentation.

91. Chakravarti, Laha, Roy. *Handbook of Methods of Applied Statistics, Volume I*. Hoboken, NJ: John Wiley and Sons; 1967.

92. Yameen B, Choi W Il, Vilos C, Swami A, Shi J, Farokhzad OC. Insight into nanoparticle cellular uptake and intracellular targeting. *J Control Release*. 2014;190:485-499.

93. Fernando LP, Kandel PK, Yu J, McNeill J, Ackroyd PC, Christensen KA. Mechanism of cellular uptake of highly fluorescent conjugated polymer nanoparticles. *Biomacromolecules*. 2010;11(10):2675-2682.

94. Delouise LA. Applications of nanotechnology in dermatology. *J Invest Dermatol*. 2012;132(3 PART 2):964-975.

95. Deng Y, Ediriwickrema A, Yang F, Lewis J, Girardi M, Saltzman WM. A sunblock based on bioadhesive nanoparticles. *Nat Mater*. 2015;14(12):1278-1285.

96. Premi S, Wallisch S, Mano CM, et al. Chemiexcitation of melanin derivatives induces DNA photoproducts long after UV exposure. *Science (80-)*. 2015;347(6224):842-847.

SUPPLEMENTAL APPENDIX

Figure S1. Sample gating for flow cytometry data shows how cell types were defined. (A) Gating of epidermal cells for viability (EMA-); myeloid lineage (CD45+); and Langerhans cells (CD45+, CD3+, MHCII-) or T-cells (CD45+, CD3-, MHCII+). (B) Gating of tumor cells for viability (EMA-) or myeloid lineage (CD45+).